

Cite this: DOI: 00.0000/xxxxxxxxxx

PoseBusters: AI-based docking methods fail to generate physically valid poses or generalise to novel sequences[†]

Martin Buttenschoen, Garrett M. Morris, and Charlotte M. Deane[‡]Received Date
Accepted Date

DOI: 00.0000/xxxxxxxxxx

The last few years have seen the development of numerous deep learning-based protein-ligand docking methods. They offer huge promise in terms of speed and accuracy. However, despite claims of state-of-the-art performance in terms of crystallographic root-mean-square deviation (RMSD), upon closer inspection, it has become apparent that they often produce physically implausible molecular structures. It is therefore not sufficient to evaluate these methods solely by RMSD to a native binding mode. It is vital, particularly for deep learning-based methods, that they are also evaluated on steric and energetic criteria. We present PoseBusters, a Python package that performs a series of standard quality checks using the well-established cheminformatics toolkit RDKit. The PoseBusters test suite validates chemical and geometric consistency of a ligand including its stereochemistry, and the physical plausibility of intra- and intermolecular measurements such as the planarity of aromatic rings, standard bond lengths, and protein-ligand clashes. Only methods that both pass these checks and predict native-like binding modes should be classed as having “state-of-the-art” performance. We use PoseBusters to compare five deep learning-based docking methods (DeepDock, DiffDock, EquiBind, TankBind, and Uni-Mol) and two well-established standard docking methods (AutoDock Vina and CCDC Gold) with and without an additional post-prediction energy minimisation step using a molecular mechanics force field. We show that both in terms of physical plausibility and the ability to generalise to examples that are distinct from the training data, no deep learning-based method yet outperforms classical docking tools. In addition, we find that molecular mechanics force fields contain docking-relevant physics missing from deep-learning methods. PoseBusters allows practitioners to assess docking and molecular generation methods and may inspire new inductive biases still required to improve deep learning-based methods, which will help drive the development of more accurate and more realistic predictions.

1 Introduction

Docking, an essential step in structure-based drug discovery¹, is the task of predicting the predominant binding modes of a protein-ligand complex given an experimentally solved or computationally modelled protein structure and a ligand structure². The predicted complexes are often used in a virtual screening workflow to help select molecules from a large library of possible candidates³; or directly by medicinal chemists to understand the binding mode and to decide whether a small molecule is a suitable drug candidate⁴.

Docking methods are designed with the understanding that binding is enabled by interactions between target and ligand structures but due to the complexity of this property methods tend to strike a balance between fast calculation and accuracy⁵.

Deep learning (DL) promises to disrupt the dominant design principle of classical docking software, and DL-based docking methods promise to unlock fast and accurate virtual screening for drug discovery. To this end, a handful of different DL-based docking methods have already been proposed^{6–10}.

Classical non-DL-based docking methods include within their search and scoring functions terms that help ensure chemical consistency and physical plausibility; for example limiting the degrees of movement in the ligand to only the rotatable bonds in the ligand and including penalties if the protein and ligand clash^{11,12}. Some current DL-based docking methods, as we will show, still lack such key “inductive biases” resulting in the creation of unrealistic poses despite obtaining root-mean-squared deviation (RMSD) values from the experimental binding mode that are less than the widely-used 2 Å threshold¹³. To assess such docking methods, an independent test suite is necessary to check the chemical consistency and physical plausibility alongside established metrics, such as the binding mode RMSD. Such a test suite would help the field to identify missing inductive biases re-

Department of Statistics, 24-29 St Giles', Oxford OX1 3LB, United Kingdom.

[†] Electronic Supplementary Information (ESI) available. See DOI: 00.0000/00000000.

[‡] Corresponding author: deane@stats.ox.ac.uk

quired to improve DL-based docking methods, driving the development of more accurate and realistic docking predictions.

The problem of assessing the physical plausibility of docking predictions is akin to the structure validation of ligand data in the Protein Data Bank (PDB)^{14,15}. Structure validation assesses the agreement of the ligands bond lengths and angles with those observed in related chemical structures and the presence of steric clashes both within the ligand and between it and its surroundings¹⁵. While these tests were designed for users to select those ligand crystal structures which are likely to be correct¹⁵, docking methods are evaluated on their ability to recover crystal structures so their output should pass the same physical plausibility tests.

Physical plausibility checks are also part of some workflows for conformation generation^{16,17}. Friedrich *et al.* use geometry checks performed by NAOMI¹⁸ which measures—like the PDB tests mention above—the deviation from known optimal values for bond lengths and bond angles, and also tests for divergences from the planarity of aromatic rings¹⁷.

In addition to physical checks, chemical checks are also needed¹⁹. Chemical checks proposed for checking PDB structures include the identification of mislabelled stereo assignment, inconsistent bonding patterns, missing functional groups, and unlikely ionisation states¹⁹. The problem of checking chemical plausibility has also come up in *de novo* molecule generation, where Brown *et al.* proposed a test suite including checks for the chemical validity of any proposed molecule²⁰. For docking, the focus is less on stability and synthetic accessibility of a molecular structure as it is hoped that these have been tested prior to attempting docking, but more on chemical consistency and physical realism of the predicted bound conformation.

Some comparisons of docking methods have included additional metrics based on volume overlap²¹ or protein-ligand interactions²² to supplement pose accuracy-based metrics such as RMSD of atomic positions and run time measurements, but the majority of comparisons of docking methods are predominantly based on binding mode RMSD^{13,23–25}.

The current standard practice of comparing docking methods based on RMSD-based metrics alone also extends to the introduction papers of recent new methods. The five DL-based docking methods we test in this paper^{6–10} all claim better performance than standard docking methods but these claims rest entirely on RMSD. None of these methods test their outputs for physical plausibility.

In this paper we present PoseBusters, a test suite that is designed to identify implausible conformations and ligand poses. We used PoseBusters to evaluate the predicted ligand poses generated by the five DL-based docking methods (DeepDock⁶, DiffDock⁷, EquiBind⁸, TankBind⁹, and Uni-Mol¹⁰) and two standard non-DL-based docking methods (AutoDock Vina¹² and Gold²⁶). These poses were generated by re-docking the cognate ligands of the 81 protein-ligand crystal complexes in the Astex Diverse set²⁷ and 308 ligands of the protein-ligand crystal complexes in the PoseBusters Benchmark set, a new set of complexes released from 2021 onwards, into their cognate receptor crystal structures. On the commonly-used Astex Diverse set, the DL-based dock-

Table 1 Selected DL-based docking methods. The selection includes five methodologically different DL-based docking methods published over the last two years.

| Method | Authors | Date | Search space |
|-----------------------|----------------------------|----------|--------------|
| DeepDock ⁶ | Méndez-Lucio <i>et al.</i> | Dec 2021 | pocket |
| DiffDock ⁷ | Corso <i>et al.</i> | Feb 2023 | blind |
| EquiBind ⁸ | Stärk <i>et al.</i> | Feb 2022 | blind |
| TANKBind ⁹ | Lu <i>et al.</i> | Oct 2022 | blind |
| Uni-Mol ¹⁰ | Zhou <i>et al.</i> | Feb 2023 | pocket |

ing method DiffDock appears to perform best in terms of RMSD alone but when taking physical plausibility into account, Gold and AutoDock Vina perform best. On the PoseBusters Benchmark set, a test set that is harder because it contains only complexes that the DL methods have not been trained on, Gold and AutoDock Vina are the best methods in terms of RMSD alone and when taking physical plausibility into account or when proteins with novel sequences are considered. The DL-based methods make few valid predictions for the unseen complexes. Overall, we show that no DL-based method yet outperforms standard docking methods when consideration of physical plausibility is taken into account. The PoseBusters test suite will enable DL method developers to better understand the limitations of current methods, ultimately resulting in more accurate and realistic predictions.

2 Methods

Five DL-based and two classical docking methods were used to re-dock known ligands into their respective proteins and the predicted ligand poses were evaluated with the PoseBusters test suite. The following section describes the docking methods, the data sets, and the PoseBusters test suite for checking physico-chemical consistency and structural plausibility of the generated poses.

2.1 Docking methods

The selected five DL-based docking methods^{6–10} cover a wide range of DL-based approaches for pose prediction. Table 1 lists the methods and their publications. In order to examine the ability of standard non-DL-based methods to predict accurate chemically and physically valid poses, we also included the well-established docking methods AutoDock Vina²⁸ and Gold²⁹.

The five DL-based docking methods can be summarised as follows. Full details of each can be found in their respective references. DeepDock⁶ learns a statistical potential based on the distance likelihood between ligand heavy atoms and points of the mesh of the surface of the binding pocket. DiffDock⁷ uses equivariant graph neural networks in a diffusion process for blind docking. EquiBind⁸ applies equivariant graph neural networks for blind docking. TankBind⁹ is a blind docking method that uses a trigonometry-aware neural network for docking in each pocket predicted by a binding pocket prediction method. Uni-Mol¹⁰ carries out docking with SE3-equivariant transformers. All five DL-based docking methods are trained on subsets of the PDB-bind General Set³⁰ as detailed in Table 2. DeepDock is trained on

Table 2 Data sets used to train the selected five machine learning-based docking methods. All five DL-based methods were trained on subsets of the PDBBind 2020 General Set.

| Method | Training and validation set |
|--------------------|--|
| DeepDock | PDBBind 2019 General Set without complexes included in CASF-2016 or those that fail pre-processing—16367 complexes |
| DiffDock, EquiBind | PDBbind 2020 General Set keeping complexes published before 2019 and without those with ligands found in test set—17347 complexes |
| TankBind | PDBbind 2020 General Set keeping complexes published before 2019 and without those failing pre-processing—18755 complexes |
| Uni-Mol | PDBBind 2020 General Set without complexes where protein sequence identity (MMSeq2) with CASF-2016 is above 40% and ligand fingerprint similarity is above 80%—18404 complexes |

v2019 and the other four are trained on v2020. It should be noted that we used the DL models as trained by the respective authors without further hyperparameter tuning.

The docking protocols that were used to generate predictions with each method and the software versions used are given in section S1 of the Supplementary Information. Table 3 lists the search space definitions that we used for each method. DeepDock and Uni-Mol require the definition of a binding site while DiffDock, EquiBind, and TankBind are ‘blind’ docking methods that search over the entire protein. We used the default search spaces for the DL-based methods but larger than default search spaces for AutoDock Vina and Gold such that they are more comparable with the blind docking DL-based methods. SI Figure S1 shows the search spaces for one example protein-ligand complex.

2.2 The PoseBusters test suite

The PoseBusters test suite is organised into three groups of tests. The first checks chemical validity and contains tests for the chemical validity and consistency relative to the input. The second group checks intramolecular properties and tests for the ligand geometry and the ligand conformation’s energy computed using the universal force field (UFF)³². The third group considers intermolecular interactions and checks for protein-ligand and ligand-cofactor clashes. Descriptions of all the tests PoseBusters performs in the three sections are listed in Table 4. Molecule poses which pass all tests in PoseBusters are ‘PB-valid’.

For evaluating docking predictions, PoseBusters requires three input files: an SDF file containing the re-docked ligands, an SDF file containing the true ligand(s), and a PDB file containing the protein with any cofactors. The three files are loaded into RDKit molecule objects with the sanitisation option turned off.

2.2.1 Chemical validity and consistency

The first test in PoseBusters checks whether the ligand passes the RDKit’s sanitisation. The RDKit’s sanitisation processes information on the valency, aromaticity, radicals, conjugation, hybridization, chirality tags, and protonation to check whether a molecule

Table 3 Search spaces of the docking methods used.

| Method | Search space |
|---------------------------------------|---|
| <i>Classical docking methods</i> | |
| Gold | Sphere of radius 25 Å centered on the geometric centre of the crystal ligand heavy atoms |
| Vina | Cube with side length 25 Å centered on the geometric centre of crystal ligand heavy atoms |
| <i>DL-based docking methods</i> | |
| DeepDock | Protein surface mesh nodes within 10 Å of any crystal ligand atom |
| Uni-Mol | Protein residues within 6 Å of any crystal ligand heavy atom |
| <i>DL-based blind docking methods</i> | |
| DiffDock | Entire crystal protein |
| EquiBind | Chains of crystal protein which are within 10 Å of any crystal ligand heavy atom |
| TankBind | Pockets identified by P2Rank ³¹ |

can be represented as an octet-complete Lewis dot structure³³. Passing the RDKit’s sanitisation is a commonly-used test for chemical validity in cheminformatics, for example in *de novo* molecular generation²⁰.

The next test in PoseBusters checks for docking-relevant chemical consistency between the predicted and the true ligands by generating ‘standard InChI’ strings³⁴ for the input and output ligands after removing isotopic information and neutralising charges by adding or removing hydrogens where possible. InChI is the *de facto* standard for molecular comparison³⁵, and the ‘standard InChI’ strings generated include the layers for the molecular formula (/), molecular bonds (/c), hydrogens (/h), net charge (/q), protons (/p), tetrahedral chirality (/t), and double bond stereochemistry (/b). Standardisation of the ligand’s protonation and charge state is needed because the stereochemistry layer is dependent on the hydrogen (/h), net charge (/q) and proton (/p) layers. These can unexpectedly change during docking even though most docking software considers the charge distribution and protonation state of a ligand as fixed^{12,36}. The normalisation protocol also removes the stereochemistry information of double bonds in primary ketimines which only depends on the hydrogen atom’s ambiguous location.

2.2.2 Intramolecular validity

The first set of physical plausibility tests in the PoseBusters test suite validates bond lengths, bond angles, and internal distances between non-covalently bound pairs of atoms in the docked ligand and against the corresponding limits in the distance bounds matrix obtained from the RDKit’s Distance Geometry module. To pass the tests, all molecular measurements must lie within the user-specified tolerances. The tolerance used throughout this manuscript is 25 % for bond lengths and bond angles and 30 % for non-covalently bound pairs of atoms e.g.: if a bond is less than 75 % of the Distance Geometry bond length lower bound,

Table 4 Description of the checks used in the PoseBusters test suite.

| Test name | Description |
|--|--|
| Chemical validity and consistency | |
| File loads | The input molecule can be loaded into a molecule object by RDKit. |
| Sanitisation | The input molecule passes RDKit's chemical sanitisation checks. |
| Molecular formula | The molecular formula of the input molecule is the same as that of the true molecule. |
| Bonds | The bonds in the input molecule are the same as in the true molecule. |
| Tetrahedral chirality | The specified tetrahedral chirality in the input molecule is the same as in the true molecule. |
| Double bond stereochemistry | The specified double bond stereochemistry in the input molecule is the same as in the true molecule. |
| Intramolecular validity | |
| Bond lengths | The bond lengths in the input molecule are within 0.75 of the lower and 1.25 of the upper bounds determined by distance geometry. |
| Bond angles | The angles in the input molecule are within 0.75 of the lower and 1.25 of the upper bounds determined by distance geometry. |
| Planar aromatic rings | All atoms in aromatic rings with 5 or 6 members are within 0.25 Å of the closest shared plane. |
| Planar double bonds | The two carbons of aliphatic carbon-carbon double bonds and their four neighbours are within 0.25 Å of the closest shared plane. |
| Internal steric clash | The interatomic distance between pairs of non-covalently bound atoms is above 0.8 of the lower bound determined by distance geometry. |
| Energy ratio | The calculated energy of the input molecule is no more than 100 times the average energy of an ensemble of 50 conformations generated for the input molecule. The energy is calculated using the UFF ³² in RDKit and the conformations are generated with ETKDgv3 followed by force field relaxation using the UFF with up to 200 iterations. |
| Intermolecular validity | |
| Minimum protein-ligand distance | The distance between protein-ligand atom pairs is larger than 0.75 times the sum of the pairs van der Waals radii. |
| Minimum distance to organic cofactors | The distance between ligand and organic cofactor atoms is larger than 0.75 times the sum of the pairs van der Waals radii. |
| Minimum distance to inorganic cofactors | The distance between ligand and inorganic cofactor atoms is larger than 0.75 times the sum of the pairs covalent radii. |
| Volume overlap with protein | The share of ligand volume that intersects with the protein is less than 7.5 %. The volumes are defined by the van der Waals radii around the heavy atoms scaled by 0.8. |
| Volume overlap with organic cofactors | The share of ligand volume that intersects with organic cofactors is less than 7.5 %. The volumes are defined by the van der Waals radii around the heavy atoms scaled by 0.8. |
| Volume overlap with inorganic cofactors | The share of ligand volume that intersects with inorganic cofactors is less than 7.5 %. The volumes are defined by the van der Waals radii around the heavy atoms scaled by 0.5. |

it is treated as anomalous. This was selected as all but one of the crystal ligands in the Astex Diverse set and all of those in the PoseBusters Benchmark set pass at this threshold.

The PoseBusters test for flatness checks that groups of atoms lie in a plane by calculating the closest plane to the atoms and checking that all atoms are within a user-defined distance from this plane. This test is performed for 5- and 6-membered aromatic rings and non-ring non-aromatic carbon-carbon double bonds. The chosen threshold of 0.25 Å admits all Astex Diverse and PoseBusters Benchmark set crystal structures by a wide margin and as with all other thresholds can be adjusted by the user.

The final test for intramolecular physicochemical plausibility carried out by PoseBusters is an energy calculation to detect unlikely conformations. Our metric for this is the ratio of the energy of the docked ligand conformation to the mean of the energies of a set of 50 generated unconstrained conformations as in Wills *et al.*³⁷. The conformations are generated using the RDKit's ETKDGv3 conformation generator³⁸ followed by a force field relaxation using the UFF³² and up to 200 iterations. The test suite rejects conformations for which this ratio is larger than a user-specified threshold. Wills *et al.* set a ratio of 7 based on the value where 95 % of the crystal ligands in the PDBbind data set are considered plausible³⁷. We selected a less strict ratio of 100 where only one structure each from the Astex Diverse and PoseBusters Benchmark set is rejected.

2.2.3 Intermolecular validity

Intermolecular interactions are evaluated by two sets of tests in the PoseBusters test suite. The first set checks the minimum distance between molecules and the second checks the share of overlapping volume. Both sets of tests report on intermolecular interactions of the ligand with four types of molecules: the protein, organic cofactors, and inorganic cofactors.

For the distance-based intermolecular tests PoseBusters calculates the ratio of the pairwise distance between pairs of heavy atoms of two molecules and the sum of the two atoms' van der Waals radii. If this ratio is smaller than a user-defined threshold then the test fails. The default threshold is 0.75 for all pairings. For inorganic cofactor-ligand pairings the covalent radii are used. All crystal structures in the Astex Diverse set and all but one in the PoseBusters Benchmark set pass at this threshold.

For the second set of intermolecular checks, PoseBusters calculates the share of the van der Waals volume of the heavy atoms of the ligand that overlaps with the van der Waals volume of the heavy atoms of the protein using the RDKit's ShapeTverskyIndex function. The tests have a configurable scaling factor for the volume-defining van der Waals radii and a threshold that defines how much overlap constitutes a clash. A threshold is necessary because many crystal structures already contain clashes. For example, Verdonk *et al.* found that 81 out of 305 selected high-quality protein-ligand complexes from the PDB contain steric clashes²⁶. The overlap threshold is 7.5 % for all molecule pairings and the scaling factor is 0.8 for protein-ligand and organic cofactor-ligand pairings and 0.5 for inorganic cofactor-ligand pairings.

2.3 Quality of fit

PoseBusters calculates the minimum heavy-atom symmetry-aware root-mean-square deviation (RMSD) between the predicted ligand binding mode and the closest crystallographic ligand using the RDKit's GetBestRMS function. Coverage, a metric often used for testing docking methods, is the share of predictions that are within a user adjustable threshold which by default is 2 Å RMSD. This value is arbitrary but commonly-used and recommended for regular-size ligands¹³.

2.4 Sequence identity

In this paper, sequence identity between two amino acid chains is the number of exact residue matches after sequence alignment divided by the number of residues of the query sequence. The sequence alignment used is the Smith–Waterman algorithm³⁹ implemented in Biopython⁴⁰ using an open gap score of -11 and an extension gap score of -1 and the BLOSUM62 substitution matrix. Unknown amino acid residues are counted as mismatches.

2.5 Molecular mechanics energy minimisation

Post-docking energy minimisation of the ligand structure in the binding pocket was performed using the AMBER ff14sb force field⁴¹ and the Sage small molecule force field⁴² in OpenMM⁴³. The protein files were prepared using PDBfixer⁴³ and all protein atom positions were fixed in space only allowing updates to the ligand atoms positions. Minimisation was performed until energy convergence within 0.01 kJ mol⁻¹.

2.6 Data

2.6.1 Astex Diverse set

The Astex Diverse set²⁷ published in 2007 is a set of hand-picked, relevant, diverse, and high-quality protein-ligand complexes from the PDB¹⁴. The complexes were downloaded from the PDB as MMTF files⁴⁴ and PyMOL⁴⁵ was used to remove solvents and all occurrences of the ligand of interest from the complexes before saving the proteins with the cofactors in PDB files and the ligands in SDF files.

2.6.2 PoseBusters Benchmark set

The PoseBusters Benchmark set is a new set of carefully-selected publicly-available crystal complexes from the PDB. It is a diverse set of recent high-quality protein-ligand complexes which contain drug-like molecules. It only contains complexes released since 2021 and therefore does not contain any complexes present in the PDBbind General Set v2020 used to train many of the methods. Table S2 lists the steps used to select the 308 unique proteins and 308 unique ligands in the PoseBusters Benchmark set. The complexes were downloaded from the PDB as MMTF files and PyMOL was used to remove solvents and all occurrences of the ligand of interest before saving the proteins with the cofactors in PDB files and the ligands in SDF files.

3 Results

The following section presents the analysis of the PoseBusters test suite on the re-docked ligands of five DL-based docking methods

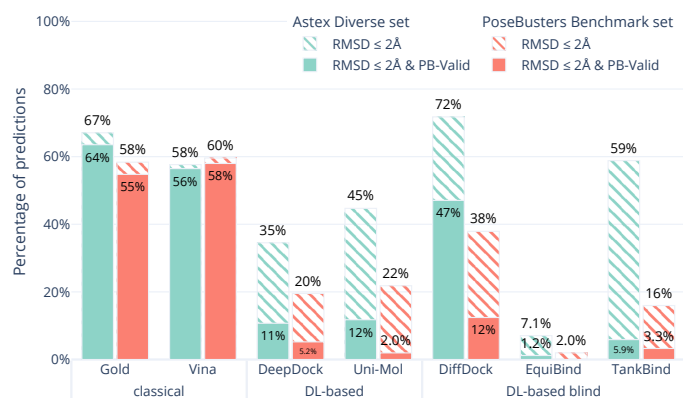


Fig. 1 Comparative performance of the docking methods. The Astex Diverse set (85 cases) was chosen as an easy test set containing many complexes the five DL-based methods were trained on while the PoseBusters Benchmark set (308 cases) was chosen to be a difficult test set containing complexes none of the methods was trained on. The striped bars show the share of predictions of each method that have an RMSD within 2 Å and the solid bars show the subset that in addition have valid geometries and energies, i.e., pass all PoseBuster tests and are therefore 'PB-Valid'. DiffDock appears to outperform the classical methods on the Astex Diverse set when only binding mode RMSD is considered (striped teal bars). However, when physical plausibility is also considered (solid teal bars) or when presented with the PoseBusters Benchmark set (coral bars), AutoDock Vina and Gold outperform all DL-based methods.

and two standard non-DL-based docking methods on the 85 ligands of the Astex Diverse set and the 308 ligands of the PoseBusters Benchmark set into the receptors crystal structures.

3.1 Results on the Astex Diverse set

Figure 1 shows the overall results of the seven (AutoDock Vina¹², Gold²⁶, DeepDock⁶, DiffDock⁷, EquiBind⁸, TankBind⁹, Uni-Mol¹⁰) docking methods on the Astex Diverse set in ocean green. The striped bars show the performance only in terms of RMSD coverage ($\text{RMSD} \leq 2 \text{ \AA}$) and the solid bars show the performance after also considering physical plausibility, i.e., only predictions which in addition pass all tests in PoseBusters and are therefore PB-valid.

The Astex Diverse set is a well-established and commonly-used benchmark for evaluating docking methods. Good performance on this set is expected because the five DL-based methods evaluated here have been trained on most of these complexes. 47 of the 81 complexes in the Astex Diverse set are in the PDBbind 2020 General Set and 67 out of the 81 of the Astex Diverse set proteins have more than 95% sequence identity with proteins found in PDBbind 2020 General Set. AutoDock Vina may also perform well on this data set because the linear regression model behind the scoring function was trained on an earlier version of PDBbind¹² which already included most of the Astex Diverse set.

The RMSD criterion alone (striped green bars in Figure 1) gives the impression that DiffDock (72%) performs better than TankBind (59%), Gold (67%), AutoDock Vina (58%) and Uni-Mol (45%). However, when we look closer, accepting only ligand binding modes that are physically sensible, i.e., those predictions that pass all PoseBusters tests and are therefore PB-valid (solid

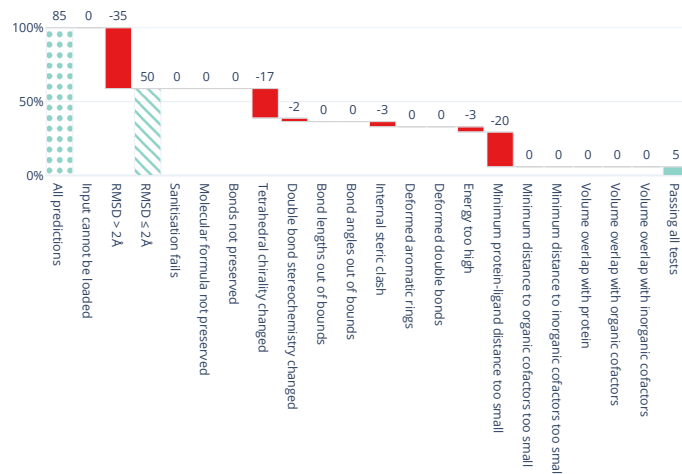


Fig. 2 Waterfall plot showing the PoseBusters tests as filters for the TankBind predictions on the Astex Diverse data set. The tests in the PoseBuster test suits are described in Table 4. The leftmost (dotted) bar shows the number of complexes in the test set. The red bars show the number of predictions that fail with each additional test going from left to right. The rightmost (solid) bar indicates the number of predictions that pass all tests, i.e. those that are 'PB-Valid'. For the 85 test cases in the Astex Diverse set 50 (59%) predictions have RMSD within 2 Å RMSD and 5 (5.9%) pass all tests. Figures S5 and S6 in the Supplementary Information show waterfall plots for all methods and both data sets.

green bars in Figure 1), many of the apparently impressive DL predictions are removed. The best three methods when considering RMSD and physical plausibility are Gold (64%), AutoDock Vina (56%), and DiffDock (47%) followed by Uni-Mol (12%), DeepDock (11%) and TankBind (5.9%). DiffDock is therefore the only DL-based method that has comparable performance to the standard methods on the Astex Diverse set when considering physical plausibility of the predicted poses.

All five DL-based docking methods struggle with physical plausibility, but even the poses produced by the classical methods Gold and AutoDock Vina do not always pass all the checks. Figure 2 shows a waterfall plot that indicates how many predicted binding modes fail each test. The waterfall plots for the remaining methods are shown in SI Figure S5. The DL-based methods fail on different tests. TankBind habitually overlooks stereochemistry, Uni-Mol very often fails to predict valid bond lengths, and EquiBind tends to produce protein-ligand clashes. The classical methods Gold and AutoDock Vina pass most tests but also generated a few protein-ligand clashes. Figure 3 shows examples of poses generated by the methods illustrating various failure modes.

The results on the Astex Diverse set suggest that despite what the $\text{RMSD} \leq 2 \text{ \AA}$ criterion would indicate, no DL-based method outperforms classical docking methods when the physical plausibility of the ligand binding mode is taken into account. However, DiffDock in particular is capable of making a large number of useful predictions.

3.2 Results on the PoseBusters Benchmark set

The results of the seven (AutoDock Vina, Gold, DeepDock, DiffDock, EquiBind, TankBind, Uni-Mol) docking methods on the

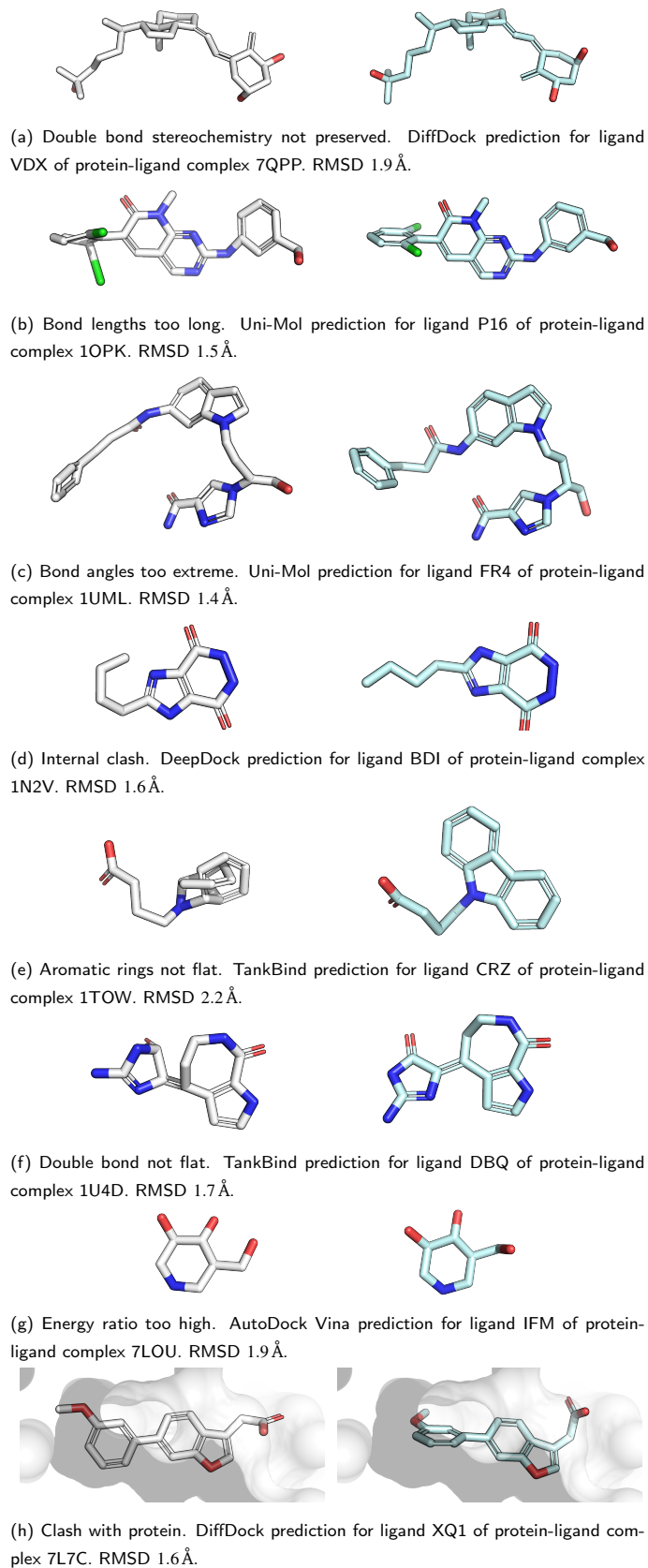


Fig. 3 Examples of failure modes that PoseBusters is able to detect. Predictions are shown on the left with white carbons and the crystal structures on the right have cyan carbons. Oxygen atoms are red, nitrogen atoms are dark blue, chlorine atoms are green. Most of the shown predictions have a RMSD within 2 Å but all are physically invalid.

PoseBusters Benchmark set are shown in coral in Figure 1. The striped bars show the performance only in terms of coverage (RMSD within 2 Å) and the solid bars show the performance in terms of PB-validity (passing all of PoseBusters tests).

The PoseBusters Benchmark set was designed to contain no complexes that are in the training data for any of the methods. Performing well on this data set requires a method to be able to generalise well.

All methods perform worse on the PoseBusters Benchmark set than the Astex Diverse set. Gold (55 %) and AutoDock Vina (58 %) perform the best out of the seven methods with (solid coral bars) and without (striped coral bars) considering PB-validity. On the PoseBusters Benchmark set, the best performing DL method, DiffDock (12 %), does not compete with the two standard docking methods. Gold and AutoDock Vina again pass the most tests but for a few protein-ligand clashes.

The waterfall plots in SI Figure S6 show which tests fail for each method on the PoseBusters Benchmark set. Again, the methods have different merits and shortcomings. Out of the five DL-based methods, DiffDock still produces the most physically valid poses but few predictions lie within the 2 Å RMSD threshold. EquiBind, Uni-Mol and TankBind generate almost no physically valid poses that pass all tests. Uni-Mol has a relatively good RMSD score (22 %) but struggles to predict planar aromatic rings and correct bond lengths.

Figure 4 shows the results of the docking methods on the PoseBusters Benchmark set but stratified by the target protein receptor's maximum sequence identity with the proteins in the PDBbind 2020 General Set³⁰. As the DL-based methods were all trained on subsets of the PDBbind 2020 General Set, this roughly quantifies how different the test set protein targets are from those that the methods were trained on. We bin the test cases into three categories low [0, 30 %], medium (30 %, 90 %], and high (90 %, 100 %) maximum percentage sequence identity. Without considering physical plausibility (striped bars), the classical methods appear to perform as well on the three protein similarity bins while the DL-based methods perform worse on the proteins with lower sequence identity. This suggests that the DL-based methods are overfitting to the protein targets in their training sets.

We also compared the performance of the docking methods on the PoseBusters Benchmark set stratified by whether protein-ligand complexes contain cofactors (SI Figure S3). Here, we loosely define cofactors as non-protein non-ligand compounds such as metal ions, iron-sulfur clusters, and organic small molecules in the crystal complex within 4.0 Å of any ligand heavy atom. About 45% of protein-ligand complexes in the PoseBusters Benchmark set have a cofactor (SI Figure S2). The classical methods perform slightly better when a cofactor is present while the DL-based docking methods perform worse on those systems.

3.3 Results with pose-docking energy minimisation

In order to examine whether the outputs of the DL-based methods can be made physically plausible we performed an additional post-docking energy minimisation of the ligand structures in the binding pocket for the PoseBusters Benchmark set (Figure 5).

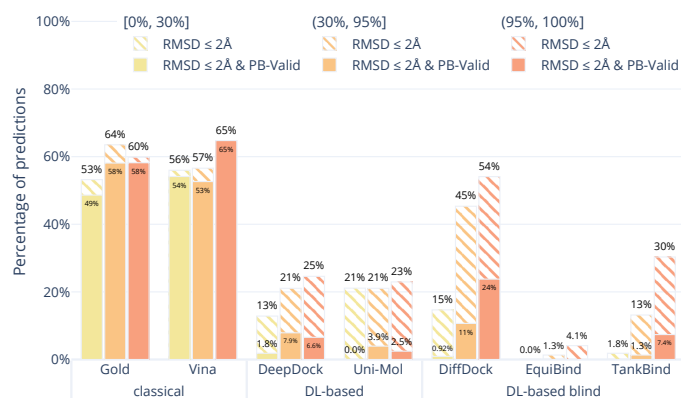


Fig. 4 Comparative performance of docking methods on the PoseBusters Benchmark set stratified by sequence identity relative to the PDBBind General Set v2020. The sequence identity is the maximum sequence identity between all chains in the PoseBuster test protein and all chains in the PDBBind General Set v2020. The striped bars show the share of predictions of each method that have an RMSD within 2 Å and the solid bars show those predictions which in addition pass all PoseBuster tests and are therefore PB-valid. The DL-based methods perform far better on proteins that are similar to those they were trained on.

Again, striped bars indicate predictions with $\text{RMSD} \leq 2 \text{ \AA}$ while solid bars indicate which of those are also PB-valid i.e., pass all PoseBusters tests. The figure shows that post-docking energy minimisation significantly increases the number of physically plausible structures of the DL-based methods DiffDock, DeepDock, TankBind, and Uni-Mol but does not improve the poses predicted by AutoDock Vina and Gold. The fact that energy minimisation is able to repair many of the DL methods predicted poses and increase coverage shows that at least some force field physics is missing from DL-based docking methods. An example of a predicted pose that was fixed is shown in Figure 6. However, even with the energy minimisation step, the best DL-based docking method DiffDock still performs worse than the classical methods Gold and AutoDock Vina.

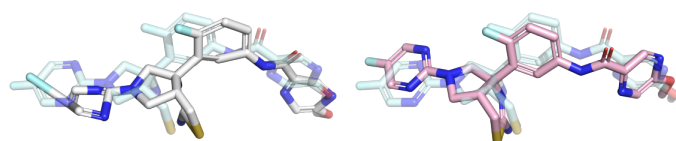


Fig. 6 Example of a prediction that was fixed by the post-docking energy minimisation. The Uni-Mol prediction ($\text{RMSD } 2.0 \text{ \AA}$) is shown in white, the optimised prediction ($\text{RMSD } 1.1 \text{ \AA}$) is shown in pink, and the crystal ligand is shown as reference in light blue. Note how the aromatic rings are flattened and the leftmost bond is shortened by the optimisation making the prediction pass all PoseBusters checks.

4 Discussion

We present PoseBusters, a test suite designed and built to identify chemically inconsistent and physically implausible ligand poses predicted by protein-ligand docking and molecular generation methods. We show the results of applying the PoseBusters test suite to the output of seven different docking methods, five current DL-based docking methods (DeepDock, DiffDock, EquiBind,

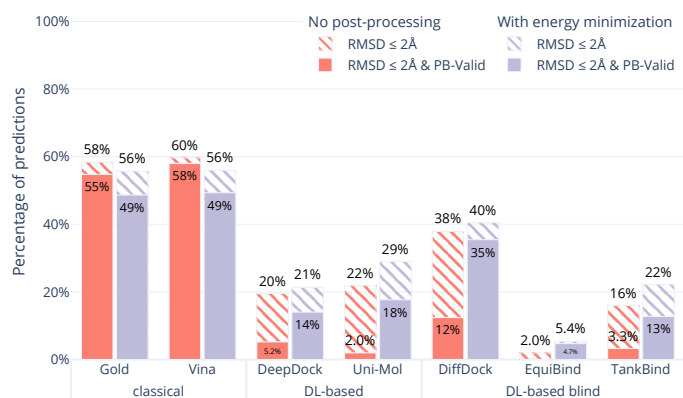


Fig. 5 Comparative performance of docking methods with post-docking energy minimisation of the ligand (while keeping the protein fixed) on the PoseBusters Benchmark set. The striped bars show the share of predictions of each method that have an RMSD within 2 Å of the crystal pose and the solid bars show those predictions which in addition pass all PoseBuster tests and are therefore PB-valid. Post-docking energy minimisation significantly improves the relative physical plausibility of the DL-based methods' predictions. This indicates that force fields contain docking-relevant physics which is missing from DL-based methods.

TankBind, and Uni-Mol) and two standard methods (AutoDock Vina and Gold).

We find that no DL-based docking method yet outperforms standard docking methods when *both* physical plausibility and binding mode RMSD is taken into account. Our work demonstrates the need for physical plausibility to be taken into account when assessing docking tools because it is possible to perform well on an RMSD-based metric while predicting physically implausible ligand poses (Figure 3). Using the tests in the PoseBusters test suite as an additional criterion when developing DL-based docking methods will help improve methods and the development of more accurate and realistic predictions.

In addition, the individual tests in the PoseBusters test suite highlight docking-relevant failure modes. The results show that Uni-Mol for example predicts non-standard bond lengths and TankBind creates internal ligand clashes. The ability to identify such failure modes in predicted ligand poses makes PoseBusters a helpful tool for developers to identify inductive biases that could improve their binding mode prediction methods.

Our results also show that, unlike classical docking methods, DL-based docking methods do not generalise well to novel data. The performance of the DL-based methods on the PoseBusters Benchmark set overall was poor and the subset of the PoseBusters Benchmark set with low sequence identity to PDBbind 2020 revealed that DL-based methods are prone to overfitting to the proteins they were trained on. Our analysis of the targets with sequence identity lower than 30% to any member of PDBbind General Set v2020 revealed that across all of the DL-based docking methods almost no physically valid poses were generated within the 2 Å threshold.

The most commonly-used train-test approach for building DL-based docking models is time-based, e.g., complexes released before a certain date are used for training and complexes released later for testing. Based on our results, we argue that this is insuf-

ficient for testing generalisation to novel targets and the sequence identity between the proteins in the training and test must be reported on.

Post-docking energy minimisation of the ligand using force fields can considerably improve the docking poses generated by DL-based methods. However, even with an energy minimisation step, the best DL-based method, DiffDock, does not outperform classical docking methods like Gold and AutoDock Vina. This shows that at least some key aspects of chemistry and physics encoded in force fields are missing from deep learning models.

The PoseBusters test suite provides a new criterion, PB-validity, beyond the traditional “RMSD $\leq 2\text{\AA}$ ” rule to evaluate the predictions of new DL-based methods, and hopefully will help to identify inductive biases needed for the field to improve docking and molecular generation methods, ultimately resulting in more accurate and realistic predictions. The next generation of DL-based docking methods should aim to outperform standard docking tools on both RMSD criteria and in terms of chemical consistency, physical plausibility, and generalisability.

Data availability

PoseBusters is made available as a pip-installable Python package and as open source code under the BSD-3-Clause license at github.com/maabuu/posebusters. Data for this paper, including the Astex Diverse set and PoseBusters Benchmark set, as well as the individual tabulated test results for each docking are available at Zenodo at <https://zenodo.org/records/8278563>.

Author Contributions

The manuscript was conceptualised and written through contributions of all authors. M. B. performed the computational experiments, created the PoseBusters software, and wrote the original draft. C. M. D. and G. M. M. supervised the work and reviewed and edited the manuscript.

Conflicts of interest

There are no conflicts to declare.

Acknowledgements

We thank Andrew Henry for bringing to our attention the ligands with crystal contacts, enhancing the quality and accuracy of the PoseBusters Benchmark set.

References

- 1 J. De Ruyck, G. Brysbaert, R. Blossey and M. Lensink, *Advances and Applications in Bioinformatics and Chemistry*, 2016, **Volume 9**, 1–11.
- 2 G. M. Morris and M. Lim-Wilby, in *Molecular Modeling of Proteins*, Humana Press, Totowa, NJ, 2008, pp. 365–382.
- 3 E. Lionta, G. Spyrou, D. Vassilatis and Z. Cournia, *Current Topics in Medicinal Chemistry*, 2014, **14**, 1923–1938.
- 4 G. Patrick, in *An Introduction to Medicinal Chemistry*, Oxford University Press, 2017, pp. 223–255.
- 5 G. Patrick, in *An Introduction to Medicinal Chemistry*, Oxford University Press, 2017, pp. 349–394.
- 6 O. Méndez-Lucio, M. Ahmad, E. A. del Rio-Chanona and J. K. Wegner, *Nature Machine Intelligence*, 2021, **3**, 1033–1039.
- 7 G. Corso, H. Stärk, B. Jing, R. Barzilay and T. Jaakkola, International Conference on Learning Representations, 2023.
- 8 H. Stärk, O. Ganea, L. Pattanaik, D. Barzilay and T. Jaakkola, International Conference on Machine Learning, 2022, pp. 20503–20521.
- 9 W. Lu, Q. Wu, J. Zhang, J. Rao, C. Li and S. Zheng, *Advances in Neural Information Processing Systems*, 2022, pp. 7236–7249.
- 10 G. Zhou, Z. Gao, Q. Ding, H. Zheng, H. Xu, Z. Wei, L. Zhang and G. Ke, International Conference on Learning Representations, 2023.
- 11 G. Jones, P. Willett and R. C. Glen, *Journal of Molecular Biology*, 1995, **245**, 43–53.
- 12 O. Trott and A. J. Olson, *Journal of Computational Chemistry*, 2009, 455–461.
- 13 J. C. Cole, C. W. Murray, J. W. M. Nissink, R. D. Taylor and R. Taylor, *Proteins: Structure, Function, and Bioinformatics*, 2005, **60**, 325–332.
- 14 H. M. Berman, *Nucleic Acids Research*, 2000, **28**, 235–242.
- 15 C. Shao, J. D. Westbrook, C. Lu, C. Bhikadiya, E. Peisach, J. Y. Young, J. M. Duarte, R. Lowe, S. Wang, Y. Rose, Z. Feng and S. K. Burley, *Structure*, 2022, **30**, 252–262.e4.
- 16 P. C. D. Hawkins, A. G. Skillman, G. L. Warren, B. A. Ellingson and M. T. Stahl, *Journal of Chemical Information and Modeling*, 2010, **50**, 572–584.
- 17 N.-O. Friedrich, C. de Bruyn Kops, F. Flachsenberg, K. Sommer, M. Rarey and J. Kirchmair, *Journal of Chemical Information and Modeling*, 2017, **57**, 2719–2728.
- 18 S. Urbaczek, A. Kolodzik, J. R. Fischer, T. Lippert, S. Heuser, I. Groth, T. Schulz-Gasch and M. Rarey, *Journal of Chemical Information and Modeling*, 2011, **51**, 3199–3207.
- 19 G. L. Warren, T. D. Do, B. P. Kelley, A. Nicholls and S. D. Warren, *Drug Discovery Today*, 2012, **17**, 1270–1281.
- 20 N. Brown, M. Fiscato, M. H. Segler and A. C. Vaucher, *Journal of Chemical Information and Modeling*, 2019, **59**, 1096–1108.
- 21 G. L. Warren, C. W. Andrews, A.-M. Capelli, B. Clarke, J. LaLonde, M. H. Lambert, M. Lindvall, N. Nevins, S. F. Semus, S. Senger, G. Tedesco, I. D. Wall, J. M. Woolven, C. E. Peishoff and M. S. Head, *Journal of Medicinal Chemistry*, 2006, **49**, 5912–5931.
- 22 A. Ciancetta, A. Cuzzolin and S. Moro, *Journal of Chemical Information and Modeling*, 2014, **54**, 2243–2254.
- 23 K. Onodera, K. Satou and H. Hirota, *Journal of Chemical Information and Modeling*, 2007, **47**, 1609–1618.
- 24 D. Plewczynski, M. Łażniewski, R. Augustyniak and K. Ginalski, *Journal of Computational Chemistry*, 2011, **32**, 742–755.
- 25 G. Bolcato, A. Cuzzolin, M. Bissaro, S. Moro and M. Sturlese, *International Journal of Molecular Sciences*, 2019, **20**, 3558.
- 26 M. L. Verdonk, J. C. Cole, M. J. Hartshorn, C. W. Murray and R. D. Taylor, *Proteins: Structure, Function, and Bioinformatics*, 2003, **52**, 609–623.
- 27 M. J. Hartshorn, M. L. Verdonk, G. Chessari, S. C. Brewerton,

- W. T. M. Mooij, P. N. Mortenson and C. W. Murray, *Journal of Medicinal Chemistry*, 2007, **50**, 726–741.
- 28 S. Forli, R. Huey, M. E. Pique, M. F. Sanner, D. S. Goodsell and A. J. Olson, *Nature Protocols*, 2016, **11**, 905–919.
- 29 G. Jones, P. Willett, R. C. Glen, A. R. Leach and R. Taylor, *Journal of Molecular Biology*, 1997, **267**, 727–748.
- 30 Z. Liu, M. Su, L. Han, J. Liu, Q. Yang, Y. Li and R. Wang, *Accounts of Chemical Research*, 2017, **50**, 302–309.
- 31 R. Krivák and D. Hoksza, *Journal of Cheminformatics*, 2018, **10**, 39.
- 32 A. K. Rappe, C. J. Casewit, K. S. Colwell, W. A. Goddard and W. M. Skiff, *Journal of the American Chemical Society*, 1992, **114**, 10024–10035.
- 33 G. Landrum, P. Tosco, B. Kelley, Ric, Sriniker, Geddeck, D. Cosgrove, R. Vianello, NadineSchneider, E. Kawashima, D. N, A. Dalke, G. Jones, B. Cole, M. Swain, S. Turk, Alexander-Savelyev, A. Vaucher, M. Wójcikowski, I. Take, D. Probst, V. F. Scalfani, K. Ujihara, G. Godin, A. Pahl, F. Berenger, JLVarjo, Jasondbiggs, Strets123 and JP, *RDKit Q3 2022 Release*, Zenodo, 2023.
- 34 S. R. Heller, A. McNaught, I. Pletnev, S. Stein and D. Tchekhovskoi, *Journal of Cheminformatics*, 2015, **7**, 1–34.
- 35 J. M. Goodman, I. Pletnev, P. Thiessen, E. Bolton and S. R. Heller, *Journal of Cheminformatics*, 2021, **13**, 40.
- 36 P. H. M. Torres, A. C. R. Sodero, P. Jofily and F. P. Silva-Jr, *International Journal of Molecular Sciences*, 2019, **20**, 4574.
- 37 S. Wills, R. Sanchez-Garcia, S. D. Roughley, A. Merritt, R. E. Hubbard, T. Dudgeon, J. Davidson, F. von Delft and C. M. Deane, *The Use of a Graph Database Is a Complementary Approach to a Classical Similarity Search for Identifying Commercially Available Fragment Merges*, 2022.
- 38 S. Riniker and G. A. Landrum, *Journal of Chemical Information and Modeling*, 2015, **55**, 2562–2574.
- 39 T. Smith and M. Waterman, *Journal of Molecular Biology*, 1981, **147**, 195–197.
- 40 P. J. A. Cock, T. Antao, J. T. Chang, B. A. Chapman, C. J. Cox, A. Dalke, I. Friedberg, T. Hamelryck, F. Kauff, B. Wilczynski and M. J. L. De Hoon, *Bioinformatics*, 2009, **25**, 1422–1423.
- 41 J. A. Maier, C. Martinez, K. Kasavajhala, L. Wickstrom, K. E. Hauser and C. Simmerling, *Journal of Chemical Theory and Computation*, 2015, **11**, 3696–3713.
- 42 S. Boothroyd, P. K. Behara, O. Madin, D. Hahn, H. Jang, V. Gapsys, J. Wagner, J. Horton, D. Dotson, M. Thompson, J. Maat, T. Gokey, L.-P. Wang, D. Cole, M. Gilson, J. Chodera, C. Bayly, M. Shirts and D. Mobley, *Development and Benchmarking of Open Force Field 2.0.0 — the Sage Small Molecule Force Field*, 2023.
- 43 P. Eastman, J. Swails, J. D. Chodera, R. T. McGibbon, Y. Zhao, K. A. Beauchamp, L.-P. Wang, A. C. Simmonett, M. P. Harrigan, C. D. Stern, R. P. Wiewiora, B. R. Brooks and V. S. Pande, *PLOS Computational Biology*, 2017, **13**, e1005659.
- 44 A. R. Bradley, A. S. Rose, A. Pavelka, Y. Valasatava, J. M. Duarte, A. Prlić and P. W. Rose, *PLOS Computational Biology*, 2017, **13**, e1005575.
- 45 Schrödinger, LLC, *The PyMOL Molecular Graphics System*, 2015.

PoseBusters

Supplementary information

Martin Buttenschoen, Garrett M. Morris, and Charlotte M. Deane

Department of Statistics, 24-29 St Giles', Oxford OX1 3LB, United Kingdom

Contents

| | |
|---|----------|
| S1 Docking protocols | 1 |
| S2 PoseBusters Benchmark set procurement | 4 |
| S3 Data sets description | 5 |
| S4 Data sets | 6 |
| S5 Energy minimisation example | 7 |
| S6 Cofactor analysis | 8 |
| S7 Detailed results | 9 |

S1 Docking protocols

The following protocols detail how the seven docking methods were used to re-dock the ligands into the crystal structures of the Astex Diverse set and the PoseBusters Benchmark set. Methods that require an initial ligand conformation were given identical starting conformations generated with the RDKit's ETKDGv3 conformer generator¹ followed by an energy minimisation using the universal force field (UFF)². All docking protocols were given receptors prepared without waters as none of the DL-based methods supports docking with waters.

AutoDock Vina

Software version Vina 1.2.3, Meeko 0.4.0, Reduce 4.9.210817, ADFRsuite 1.0, RDKit 2022.09.1

Ligand preparation The initial ligand conformations described above were prepared with Meeko using standard settings.

Protein preparation Hydrogen atoms were added with reduce and then the PDBQT files were generated with the ADFR `prepare_receptor` script.

Parameters A bounding box with side-length 25 Å was created around the centroid of the crystal ligand. Vina was used to create 40 poses with an exhaustiveness setting of 32 and the top-ranked pose was selected.

CCDC Gold

Software version CCDC Python API version 3.0.14

Ligand preparation The initial ligand conformations described above were prepared with `LigandPreparation` using the default settings which include adding missing hydrogens, removing unknown atoms, and rule-based protonation of the ligand.

Protein preparation The protein and co-factors were loaded from separate files and all hydrogens were added.

Parameters A settings file was created for each complex using the `Docker` class default settings. The binding site was defined around the crystal ligand using `BindingSiteFromLigand` with radius 25 Å. The settings used are rescore function 'plp', autoscale 10, and early termination off. After generating 40 poses only the top-ranked pose was saved.

arXiv:2308.05777v2 [q-bio.QM] 6 Nov 2023

DeepDock

Software version DeepDock commit hash `54a2a64` from authors' public code repository <https://github.com/OptiMaL-PSE-Lab/DeepDock>, MSMS 2.6.1, PDB2PQR 2.1.1, APBS 3.4.1

Ligand preparation The generated starting ligand conformations were used without further processing.

Protein preparation The steps in example notebook `Docking_example.ipynb` were used to generate protein surface meshes. The function `compute_inp_surface` generated binding site surfaces using the crystal ligands and the crystal protein structures with a distance threshold of 10 Å.

Parameters The protocol and settings in notebook `Docking_example.ipynb` in the DeepDock repository were used for docking.

DiffDock

Software version DiffDock commit hash `fff8f0b` from authors' public code repository <https://github.com/gcorso/DiffDock>

Ligand preparation The generated starting ligand conformations were used without further processing.

Protein preparation ESM was used to generate FASTA files.

Parameters The protocol in `README.md` was used to generate ESM embeddings and then to do inference. 40 poses were sampled using 20 inference steps with no noise on the final step. The top-ranked pose was selected.

EquiBind

Software version EquiBind commit hash `41bd00f` from authors' public code repository <https://github.com/HannesStark/EquiBind>, Reduce 3.3.160602, Open Babel 3.1.0, RDKit 2022.09.1

Ligand preparation The generated starting ligand conformations were processed with Open Babel and then with the RDKit to add missing hydrogens.

Protein preparation The receptors were processed with Open Babel. Then reduce was used to correct receptor residues and to add hydrogens. Then the protein chains which have at least one residue within 10 Å of the crystal ligand were selected.

Parameters The configuration file `configs_clean/inference.yml` in the repository was used.

TankBind

Software version TANKBind commit hash `804e9fc` from authors' public code repository <https://github.com/luwei0917/TankBind>, p2rank 2.3

Ligand preparation The notebook `prediction_example_using_PDB_6hd6.ipynb` was used to renumber the ligand atoms and generate features from the ligands.

Protein preparation The notebook `prediction_example_using_PDB_6hd6.ipynb` was used to generate features from the crystal protein structures.

Parameters The steps in the notebook `prediction_example_using_PDB_6hd6.ipynb` were used for inference. The steps are running p2rank to generate a list of binding pockets and then docking using the TankBind model.

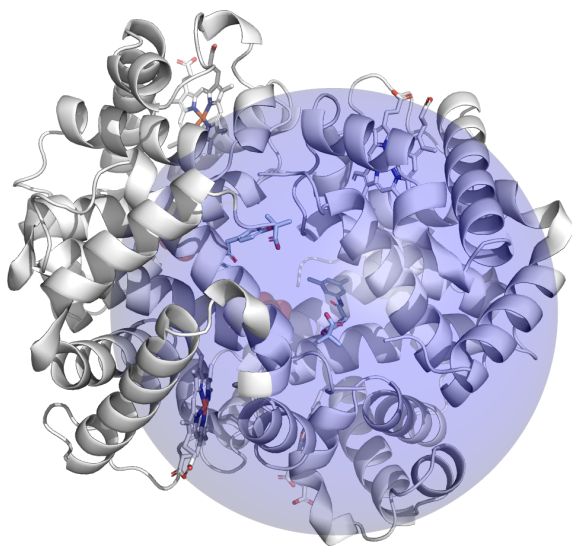
Uni-Mol

Software version Uni-Mol commit hash `b962451` from authors' public code repository <https://github.com/dptech-corp/Uni-Mol>

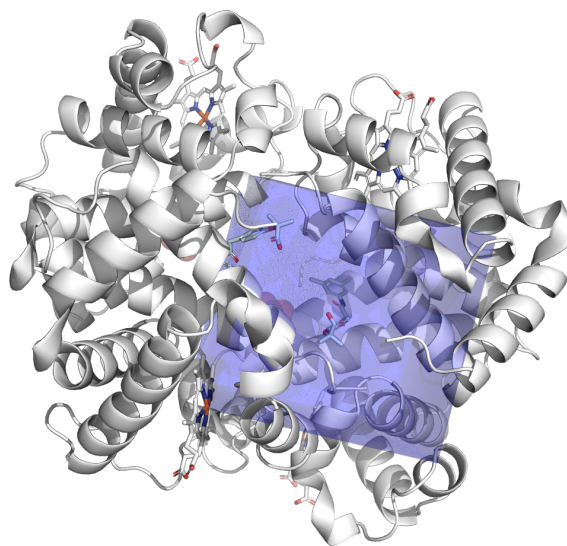
Ligand preparation The ligands were generated according to the protocol described in the `README.md` file in the top folder of the Uni-Mol repository.

Protein preparation The binding pockets residues are those within 6 Å of any crystal ligand heavy atom.

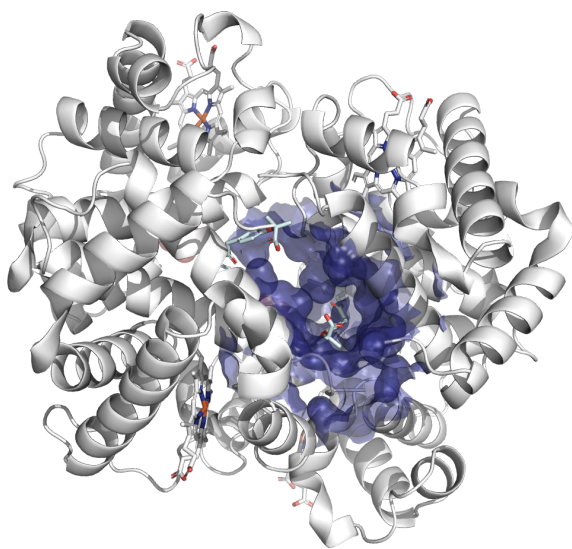
Parameters The default arguments (`recycling=3`, `batch_size=8`, `dist_threshold=8.0`) were used.



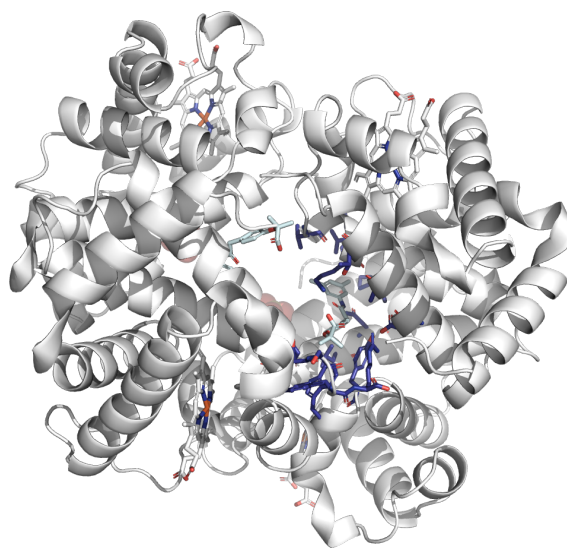
(a) Gold: Sphere of radius 25 Å centered on the geometric centre of the crystal ligand heavy atoms.



(b) AutoDock Vina: Cube with side length 25 Å centered on the geometric centre of crystal ligand heavy atoms.



(c) DeepDock: Protein surface mesh nodes within 10 Å of any crystal ligand atom.



(d) Uni-Mol: Protein residues within 6 Å of any crystal ligand heavy atom.

Figure S1: Search spaces of the docking methods illustrated on PDB entry 1G9V for ligand RQ3. The search spaces for the blind docking methods DiffDock, EquiBind, and TankBind are the entire protein crystal structure. For more information refer to Table 3 in the main text.

S2 PoseBusters Benchmark set procurement

Table S1: Selection process of the PDB entries and ligands for the PoseBusters Benchmark set. The filters are based on the PDB meta data, the PDB quality reports, and the PDB structure data. The final PoseBusters Benchmark set consists of 308 unique PDB entries containing 308 unique ligands.

| Selection step | Number of proteins (unique PDB IDs) | Number of ligands (unique CCD IDs) |
|---|--|---------------------------------------|
| PDB entries with a protein and 'ligand of interest' released from 1 January 2021 to 30 May 2023 | 10537 | 6635 |
| Ligands weighing from 100 Da to 900 Da | 10537 | 6424 |
| Ligands with at least 3 heavy atoms | 10537 | 6374 |
| Ligands containing only H, C, O, N, P, S, F, Cl atoms | 10537 | 6271 |
| Ligands that are not covalently bound to protein | 7247 | 4891 |
| Structures with no unknown atoms (e.g. element X) | 7218 | 4881 |
| X-ray structure high resolution limit at most 2 Å | 4686 | 3314 |
| Ligand real space R-factor is at most 0.2 | 3800 | 2572 |
| Ligand real space correlation coefficient is at least 0.95 | 1849 | 1054 |
| Ligand model completeness is 100% | 1820 | 1039 |
| Ligand starting conformation could be generated with ETKDGv3 ³ | 1733 | 1019 |
| All ligand SDF files can be loaded with RDKit ⁴ and pass its sanitization | 1706 | 994 |
| PDB ligand report does not list stereochemical errors | 1706 | 994 |
| PDB ligand report does not list any atomic clashes | 1256 | 844 |
| Select single protein-ligand conformation ¹ | 1256 | 844 |
| Intermolecular distance between the ligand(s) of interest and the protein is at least 0.2 Å | 1237 | 834 |
| Intermolecular distance between ligand(s) of interest and other small organic molecules is at least 0.2 Å | 1237 | 834 |
| Intermolecular distance between the ligand(s) of interest and ion metals in complex is at least 0.2 Å | 1232 | 832 |
| Blocklist for PDB entries ² | 1227 | 827 |
| Blocklist for CCD entries ³ | 1223 | 823 |
| Randomly select PDB entries to get a set with unique ligands | 809 | 823 |
| Randomly select ligands to get a set with unique PDB entries | 809 | 809 |
| Select representative PDB entries by clustering protein sequences ⁴ | 428 | 428 |
| Remove ligands which are within 5.0 Å of any protein symmetry mate | 308 | 308 |

¹ The first conformation containing the ligand of interest was chosen when multiple conformations containing the ligand were available in the PDB entry.

² The blocklist for the PDB entries (by PDB identifier) contains entries removed due to bad ligand conformations (7X48, 7UYC), ligands forming polymers (7WJD, 7DB4), racemic mixtures of ligands where the stereoisomer has a different CCD identifier (6ZYU, 7W2W), and structures containing elements Te and Yb which AutoDock Vina does not support by default (7ZSQ, 8AVA).

³ The blocklist for the ligands (by CCD identifier) contains the four entries I8P, 5A3, U71, and UEV. These four are omitted because they are highly symmetric and the substructure search yields many possible atom-atom mappings between conformations negatively affecting the RMSD calculation time.

⁴ Clustering with Diamond⁵ is done with an identity cutoff for the clustering of 0% and a minimum coverage of the cluster member sequences by the representative sequences of 100% and otherwise default values which includes the BLOSUM62 substitution matrix.

S3 Data sets description

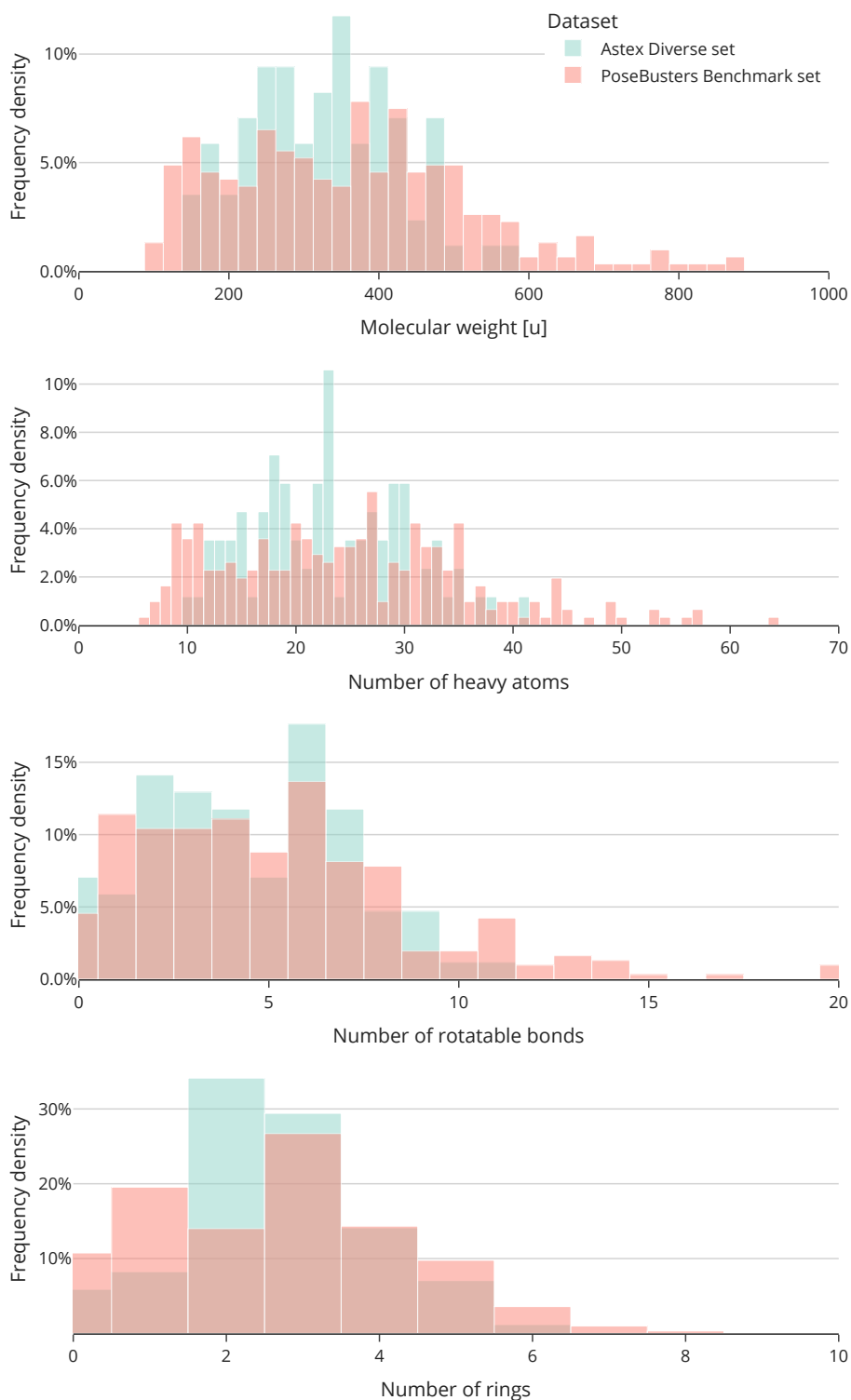


Figure S2: Comparison of the 85 ligands in the Astex Diverse set and the 308 ligands in the PoseBusters Benchmark set in terms of molecular weight, number of heavy atoms, number of rotatable bonds, and number of rings.

S4 Data sets

The following sections list the protein database⁶ (PDB) codes and chemical component dictionary⁷ (CCD) codes for the protein-ligand complexes and the corresponding ligands of interest for the two data sets used.

Astex Diverse set

1G9V RQ3, 1GKC NFH, 1GM8 SOX, 1GPK HUP, 1HNN SKF, 1HP0 AD3, 1HQ2 PH2, 1HVY D16, 1HWI 115, 1HWW SWA, 1IA1 TQ3, 1IG3 VIB, 1J3J CP6, 1JD0 AZM, 1JJE BYS, 1JLA TNK, 1K3U IAD, 1KE5 LS1, 1KZK JE2, 1L2S STC, 1L7F BCZ, 1LPZ CMB, 1LRH NLA, 1M2Z DEX, 1MEH MOA, 1MMV 3AR, 1MZC BNE, 1N1M A3M, 1N2J PAF, 1N2V BDI, 1N46 PFA, 1NAV IH5, 1OF1 SCT, 1OF6 DTY, 1OPK P16, 1OQ5 CEL, 1OWE 675, 1OYT FSN, 1P2Y NCT, 1P62 GEO, 1PMN 984, 1Q1G MTI, 1Q41 IXM, 1Q4G BFL, 1R1H BIR, 1R55 097, 1R58 AO5, 1R90 FLP, 1S19 MC9, 1S3V TQD, 1SG0 STL, 1SJ0 E4D, 1SQ5 PAU, 1SQN NDR, 1T40 ID5, 1T46 STI, 1T9B 1CS, 1TOW CRZ, 1TT1 KAI, 1TZ8 DES, 1U1C BAU, 1U4D DBQ, 1UML FR4, 1UNL RRC, 1UOU CMU, 1V0P PVB, 1V48 HA1, 1V4S MRK, 1VCJ IBA, 1W1P GIO, 1W2G THM, 1X8X TYR, 1XM6 5RM, 1XOQ ROF, 1XOZ CIA, 1Y6B AAX, 1YGC 905, 1YQY 915, 1YV3 BIT, 1YVF PH7, 1YWR LI9, 1Z95 198, 2BM2 PM2, 2BR1 PFP, 2BSM BSM

PoseBusters Benchmark set

5SAK ZRY, 5SB2 1K2, 5SD5 HWI, 5SIS JSM, 6M2B EZO, 6M73 FNR, 6T88 MWQ, 6TW5 9M2, 6TW7 NZB, 6VTA AKN, 6WTN RXT, 6XBO 5MC, 6XCT 478, 6XG5 TOP, 6XHT V2V, 6XM9 V55, 6YJA 2BA, 6YMS OZH, 6YQV 8K2, 6YQW 82I, 6YR2 T1C, 6YRV PJ8, 6YSP PAL, 6YT6 PKE, 6YYO Q1K, 6Z0R Q4H, 6Z14 Q4Z, 6Z1C 7EY, 6Z2C Q5E, 6Z4N Q7B, 6ZAE ACV, 6ZC3 JOR, 6ZCY QF8, 6ZK5 IMH, 6ZPB 3D1, 7A1P QW2, 7A9E R4W, 7A9H TPP, 7AFX R9K, 7AKL RK5, 7AN5 RDH, 7B2C TP7, 7B94 ANP, 7BCP GCO, 7BJJ TVW, 7BKA 4JC, 7BMI U4B, 7BNH BEZ, 7BTT F8R, 7C0U FGO, 7C3U AZG, 7C8Q DSG, 7CD9 FVR, 7CIJ G0C, 7CL8 TES, 7CNQ G8X, 7CNS PMV, 7CTM BDP, 7CUO PHB, 7D5C GV6, 7D6O MTE, 7DKT GLF, 7DQL 4CL, 7DUA HJ0, 7E4L MDN, 7EBG J0L, 7ECR SIN, 7ED2 A3P, 7ELT TYM, 7EPV FDA, 7ES1 UDP, 7F51 BA7, 7F5D EUO, 7F8T FAD, 7FB7 8NF, 7FHA ADX, 7FRX O88, 7FT9 4MB, 7JG0 GAR, 7JHQ VAJ, 7JMV 4NC, 7JXX VP7, 7JY3 VUD, 7K0V VQP, 7KB1 WBJ, 7KC5 BJZ, 7KM8 WPD, 7KQU YOF, 7KRU ATP, 7KZ9 XN7, 7L00 XCJ, 7L03 F9F, 7L5F XNG, 7L7C XQ1, 7LCU XTA, 7LEV 0JO, 7LJN GTP, 7LMO NYO, 7LOE Y84, 7LOU IFM, 7LT0 ONJ, 7LZD YHY, 7M31 TDR, 7M3H YPV, 7M6K YRJ, 7MFP Z7P, 7MGT ZD4, 7MGY ZD1, 7MMH ZJY, 7MOI HPS, 7MSR DCA, 7MWN WI5, 7MWU ZPM, 7MY1 IPE, 7MYU ZR7, 7N03 ZRP, 7N4N 0BK, 7N4W P4V, 7N6F 0I1, 7N7B T3F, 7N7H CTP, 7NF0 BYN, 7NF3 4LU, 7NFB GEN, 7NGW UAW, 7NLV UJE, 7NP6 UK8, 7NPL UKZ, 7NR8 UOE, 7NSW HC4, 7NU0 DCL, 7NUT GLP, 7NXO UU8, 7O0N CDP, 7O1T 5X8, 7ODY DGI, 7OEO V9Z, 7OFF VCB, 7OFK VCH, 7OLI 8HG, 7OMX CNA, 7OP9 06K, 7OPG 06N, 7OSO 0V1, 7OZ9 NGK, 7OZC G6S, 7P1F KFN, 7P1M 4IU, 7P2I MFU, 7P4C 5OV, 7P5T 5YG, 7PGX FMN, 7PIH 7QW, 7PJQ OWH, 7PK0 BYC, 7PL1 SFG, 7POM 7VZ, 7PRI 7TI, 7PRM 81I, 7PT3 3KK, 7PUV 84Z, 7Q25 8J9, 7Q27 8KC, 7Q2B M6H, 7Q5I I0F, 7QE4 NGA, 7QF4 RBF, 7QFM AY3, 7QGP DJ8, 7QHG T3B, 7QHL D5P, 7QPP VDX, 7QTA URI, 7R3D APR, 7R59 I5F, 7R6J 2I7, 7R7R AWJ, 7R9N F97, 7RC3 SAH, 7RH3 59O, 7RKW 5TV, 7RNI 60I, 7ROR 69X, 7ROU 66I, 7RSV 7IQ, 7RWS 4UR, 7RZL NPO, 7SCW GSP, 7SDD 4IP, 7SFO 98L, 7SIU 9ID, 7SUC COM, 7SZA DUI, 7T0D FPP, 7T1D E7K, 7T3E SLB, 7TB0 UD1, 7TBU S3P, 7TE8 P0T, 7TH4 FFO, 7THI PGA, 7TM6 GPJ, 7TOM 5AD, 7TS6 KMI, 7TSF H4B, 7TUO KL9, 7TXK LW8, 7TYP KUR, 7U0U FK5, 7U3J L6U, 7UAS MBU, 7UAW MF6, 7UJ4 OQ4, 7UJ5 DGL, 7UJF R3V, 7ULC 56B, 7UMW NAD, 7UQ3 O2U, 7USH 82V, 7UTW NAI, 7UXS OJC, 7UY4 SMI, 7UYB OK0, 7V14 ORU, 7V3N AKG, 7V3S 5I9, 7V43 C4O, 7VB8 STL, 7VBU 6I4, 7VC5 9SF, 7VKZ NOJ, 7VQ9 ISY, 7VWF K55, 7VYJ CA0, 7W05 GMP, 7W06 ITN, 7WCF ACP, 7WDT NGS, 7WJB BGC, 7WKL CAQ, 7WL4 JFU, 7WPW F15, 7WQQ 5Z6, 7WUX 6OI, 7WUY 76N, 7WY1 D0L, 7X5N 5M5, 7X9K 8OG, 7XBV APC, 7XFA D9J, 7XG5 PLP, 7XI7 4RI, 7XJN NSD, 7XPO UPG, 7XQZ PPF, 7XRL FWK, 7YZU DO7, 7Z1Q NIO, 7Z2O IAJ, 7Z7F IF3, 7ZCC OGA, 7ZDY 6MJ, 7ZF0 DHR, 7ZHP IQY, 7ZL5 IWE, 7ZOC T8E, 7ZTL BCN, 7ZU2 DHT, 7ZXV 45D, 7ZZW KKW, 8A1H DLZ, 8A2D KXY, 8AAU LH0, 8AEM LVF, 8AIE M7L, 8AP0 PRP, 8AQL PLG, 8AUH L9I, 8AY3 OE3, 8B8H OJQ, 8BOM QU6, 8BTI RFO, 8C3N ADP, 8C5M MTA, 8CNH V6U, 8CSD C5P, 8D19 GSH, 8D39 QDB, 8D5D 5DK, 8DHG T78, 8DKO TFB, 8DP2 UMA, 8DSC NCA, 8EAB VN2, 8EX2 Q2Q, 8EXL 799, 8EYE X4I, 8F4J PHO, 8F8E XJI, 8FAV 4Y5, 8FLV ZB9, 8FO5 Y4U, 8G0V YHT, 8G6P API, 8GFD ZHR, 8HFN XGC, 8H00 3ZI, 8SLG G5A

S5 Energy minimisation example

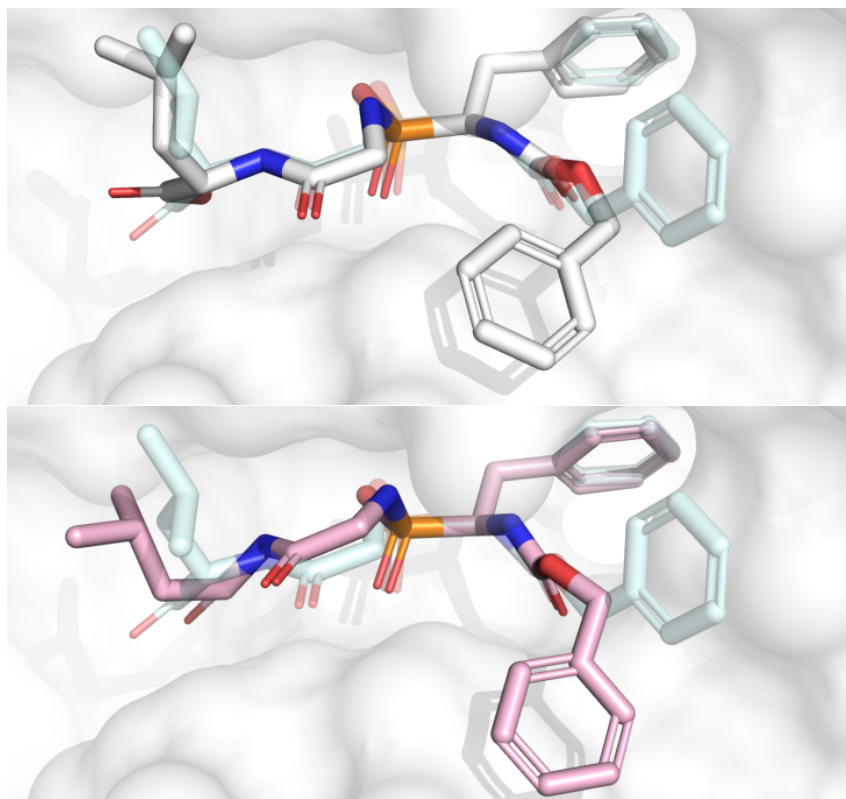


Figure S3: Example of a prediction that was ‘destroyed’ by the energy minimisation. The prediction by Autodock Vina passes all PoseBusters checks and has a RMSD of 1.9 Å and is shown in white, the optimised predicted ligand has a RMSD of 2.2 Å and is shown in pink, and the crystal ligand is shown in light blue.

S6 Cofactor analysis

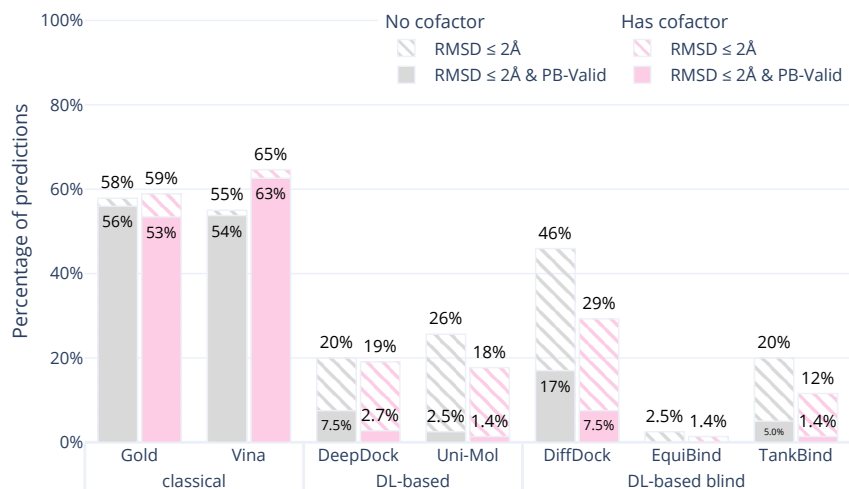


Figure S4: Comparative performance of docking methods on the PoseBusters Benchmark set stratified by the presence of cofactors. Cofactors are loosely defined as non-protein non-ligand compounds such as metal ions, iron-sulfur clusters, and organic small molecules that are within 4.0 Å of any ligand heavy atom. The striped bars show the share of predictions of each method that have an RMSD within 2 Å and the solid bars show those predictions which in addition pass all PoseBuster tests and are therefore PB-valid. The classical docking methods perform better on those systems with cofactors present while the DL-based methods perform worse on those systems.

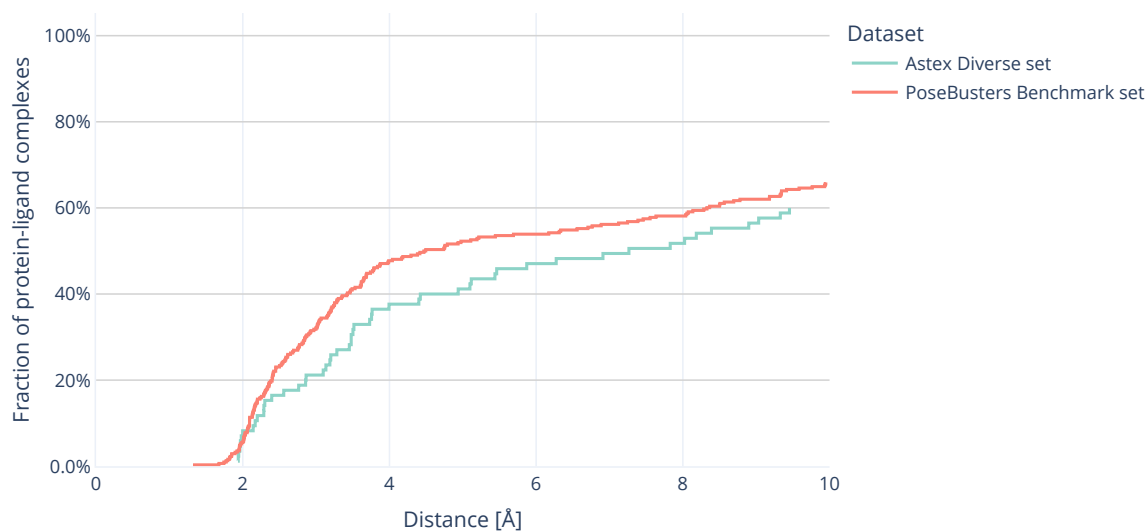


Figure S5: Fraction of protein-ligand complexes with a cofactor close to the ligand as a function of the distance threshold used. Here a cofactor is any other compound present in the crystal structure besides the ligand of interest, the protein and solvent. This includes metal ions, iron-sulfur clusters, and small organic molecules. 46% of the protein-ligand complexes in the PoseBusters Benchmark set have a cofactor within 4 Å of the ligand.

S7 Detailed results

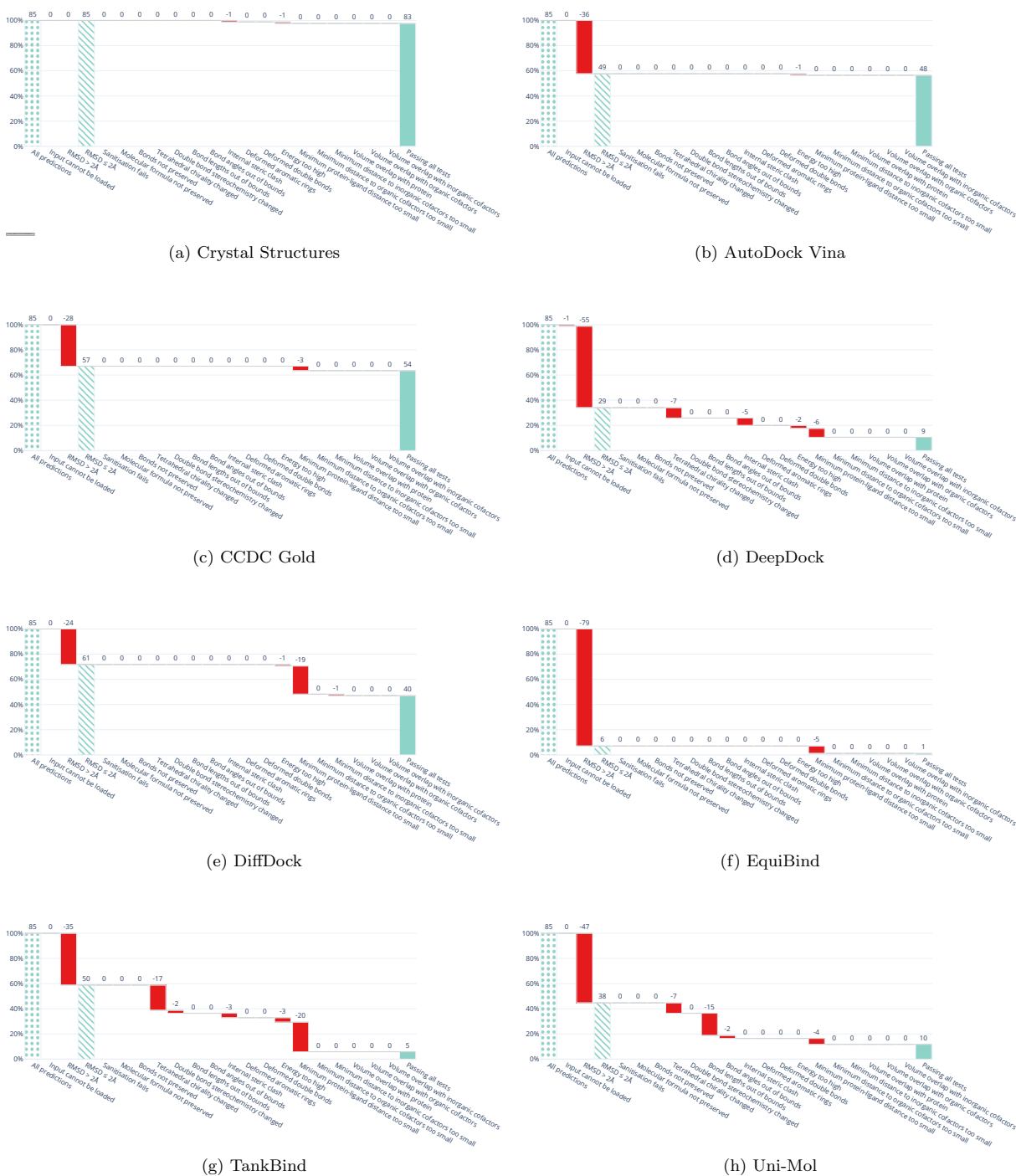


Figure S6: Waterfall plots showing test results for the Astex Diverse set. The leftmost (dotted) bars show the number of complexes in the test set. The red bars show the number of predictions that fail with each additional test going from left to right. The right most (solid) bar indicates the number of predictions that pass all tests. As a reading example, panel (a) shows that out of AutoDock Vina's 85 predictions 37 are not within 2 angstrom RMSD and one additional prediction fails the energy ratio check so that overall 47 ligands have a low RMSD and pass all tests. AutoDock Vina and CCDC Gold pass the most tests.

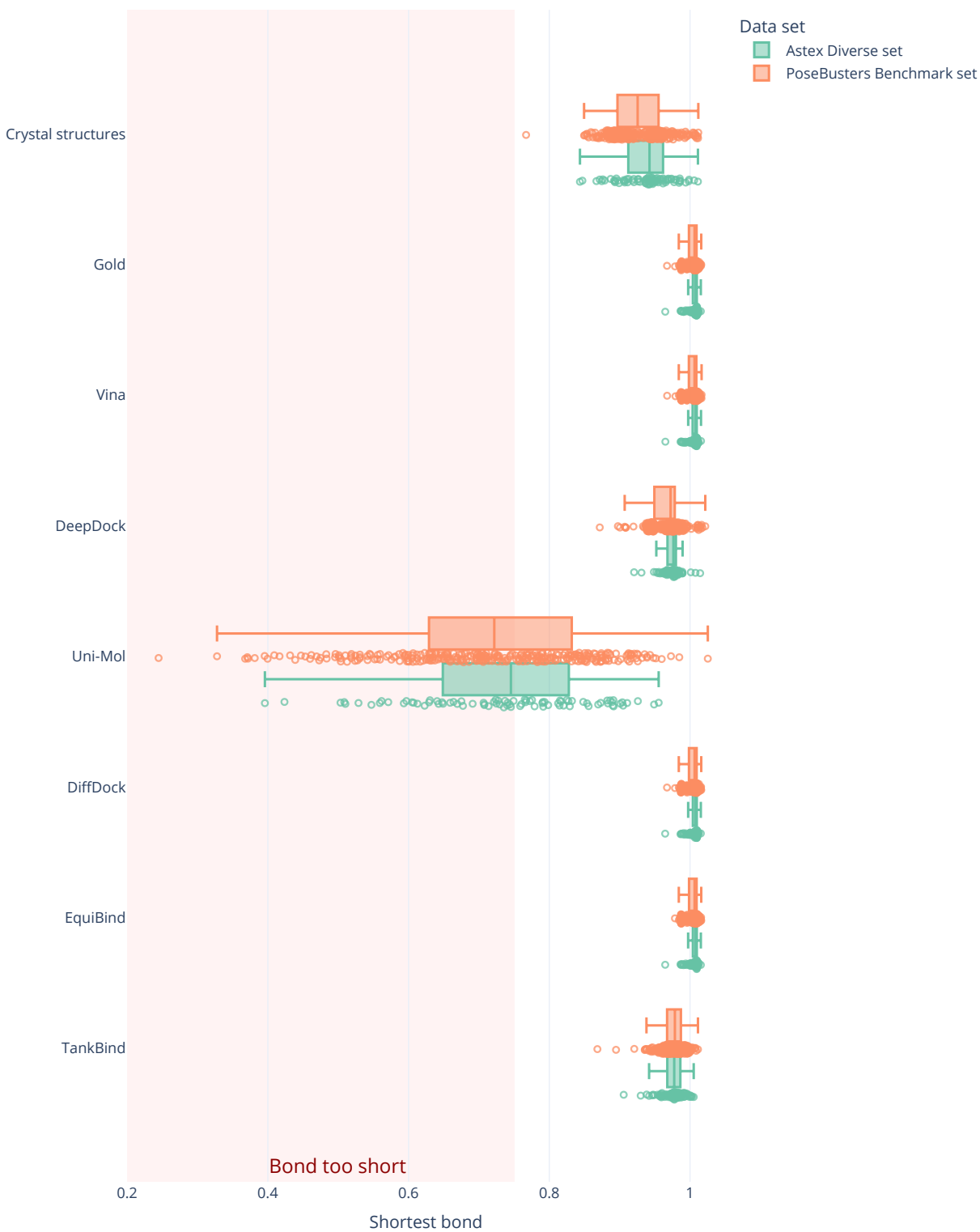


Figure S8: Distribution of shortest bond lengths. Shown are the relatively shortest bonds of each predicted ligand for each method and data set. The bond length is normalized by the lower bound for bond length obtained from Distance Geometry (DG). The lower bound correspond to one. A dot to the left of 0.75 indicates that the relatively shortest bond was more than 25% shorter than the DG lower bound. All methods except TankBind and Uni-Mol take the bond lengths from the provided ligand starting conformation. Uni-Mol and TankBind generate the bond lengths.



Figure S9: Distribution of longest bond lengths. Shown are the relatively longest bonds of each predicted ligand for each method and data set. The bond length is normalized by the upper bound for bond length obtained from Distance Geometry (DG). The upper bound correspond to one. A dot to the right of 1.25 indicates that the relatively shortest bond was more than 25% longer than the DG upper bound. All methods except TankBind and Uni-Mol take the bond lengths from the provided ligand starting conformation. Uni-Mol and TankBind generate the bond lengths.



Figure S10: Distribution of relative bond angles. Shown are the most extreme angles of each predicted ligand for each method and data set. Each bond angle is normalized by the corresponding bond length bounds obtained from Distance Geometry (DG). The upper bound corresponds to one. A dot to the right of 1.25 indicates that an angle is more than 25% larger or shorter than the DG bounds permit. All methods except TankBind and Uni-Mol take the bond angles from the provided ligand starting conformation. Uni-Mol and TankBind generate the angles.

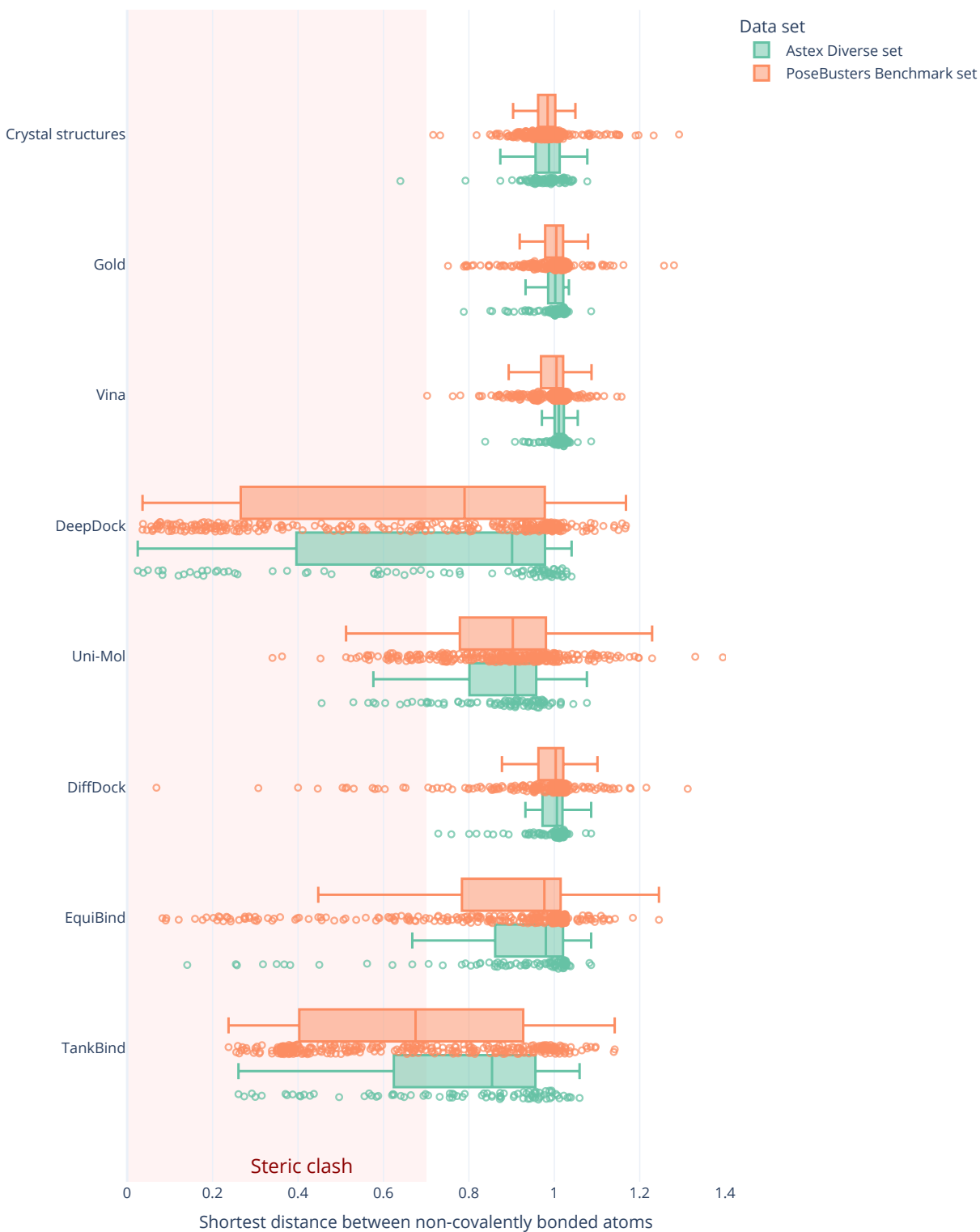


Figure S11: Distribution of distances between unbounded atoms. The distribution shows the closest pair of unbounded atoms in each predicted ligand for each method and data set. Each distance is normalized to the Distance Geometry bounds. The lower bound corresponds to one. A dot to the left of 0.7 indicates that a distance was more than 30% shorter than the lower bound and was counted as a clash.

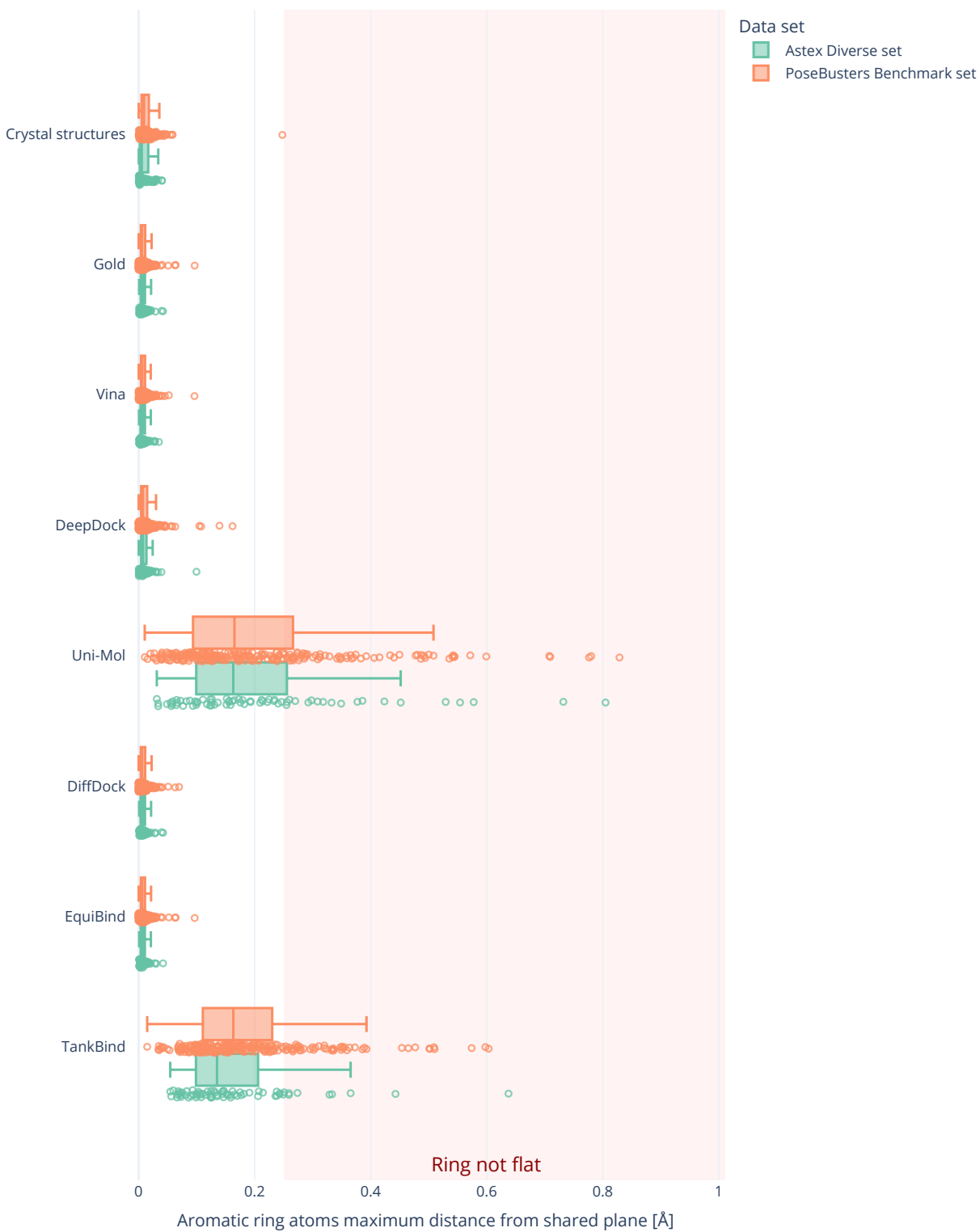


Figure S12: Distance from shared plane of atoms in 5- or 6-membered aromatic rings. The largest distance in Angstrom from the shared plane is shown for each protein ligand complex. If a ligand has no rings it is not shown. TankBind and Uni-Mol generate non-flat rings.

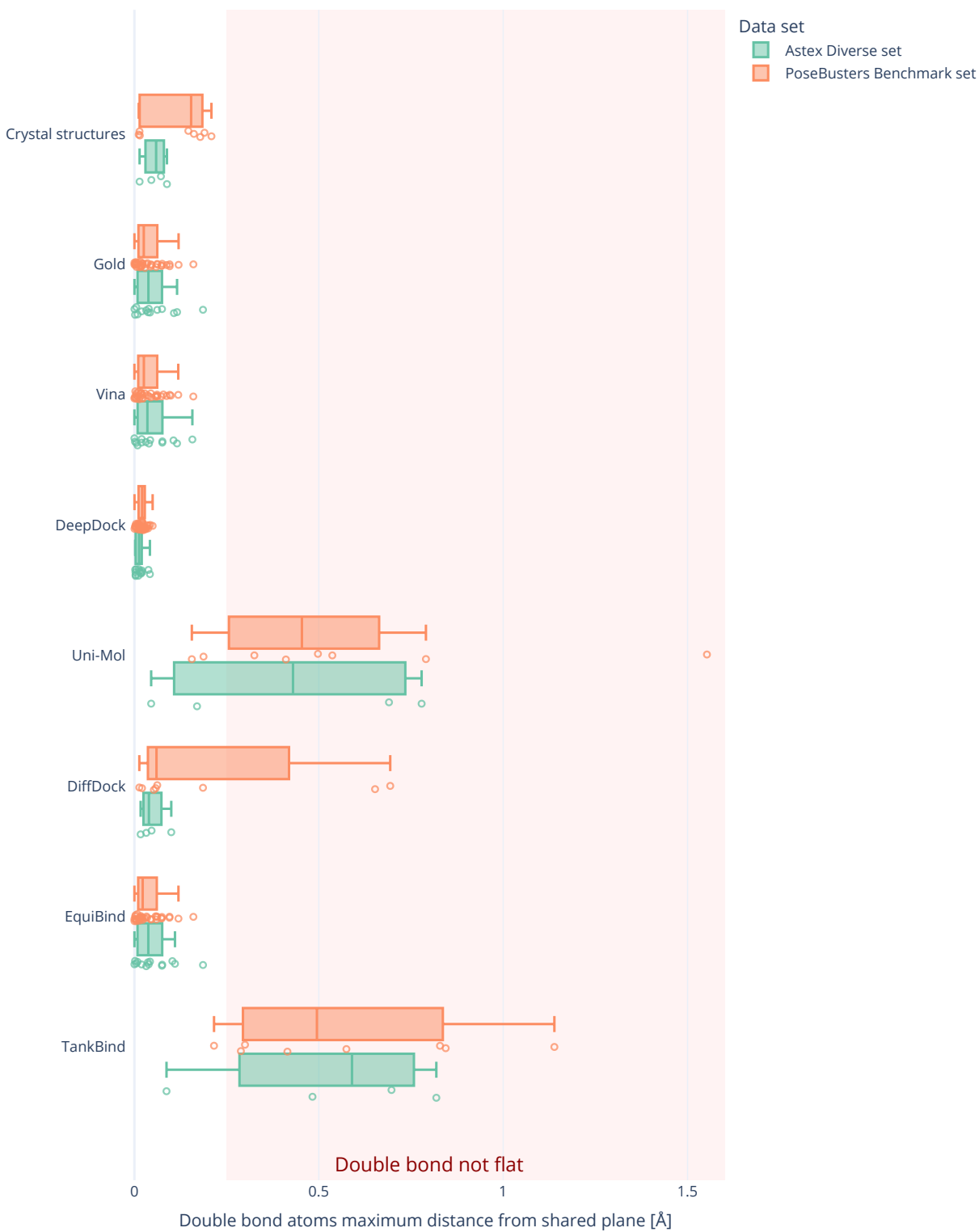


Figure S13: Distance from shared plane of atoms around aliphatic carbon-carbon double bonds. The largest distance in Angstrom from the shared plane of the two carbons and their four neighbours is shown for each protein ligand complex. If a ligand has no aliphatic carbon-carbon double bonds it is not shown. TankBind and Uni-Mol generate non-flat double bonds.

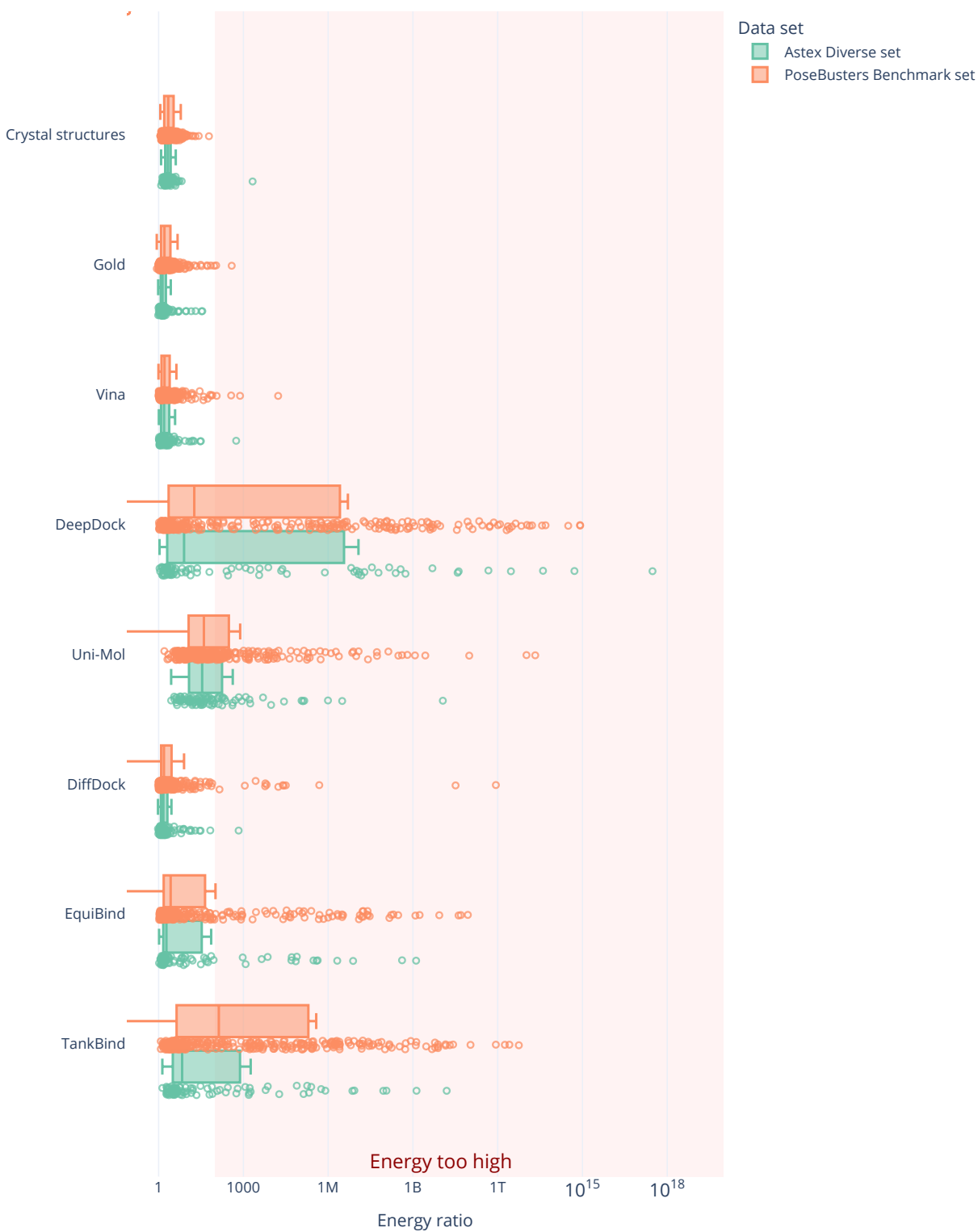


Figure S14: Energy ratio distributions. The ratio is the energy of the predicted ligand conformation over the average energy of an ensemble of 50 conformations generated with ETKDGv3. The UFF implemented in RDKit was used. The dashed red line shows the cutoff value of 100. There is only one crystal ligand in each data set with a higher energy ratio than the cutoff but all docking methods generate multiple high energy conformations above the cutoff.

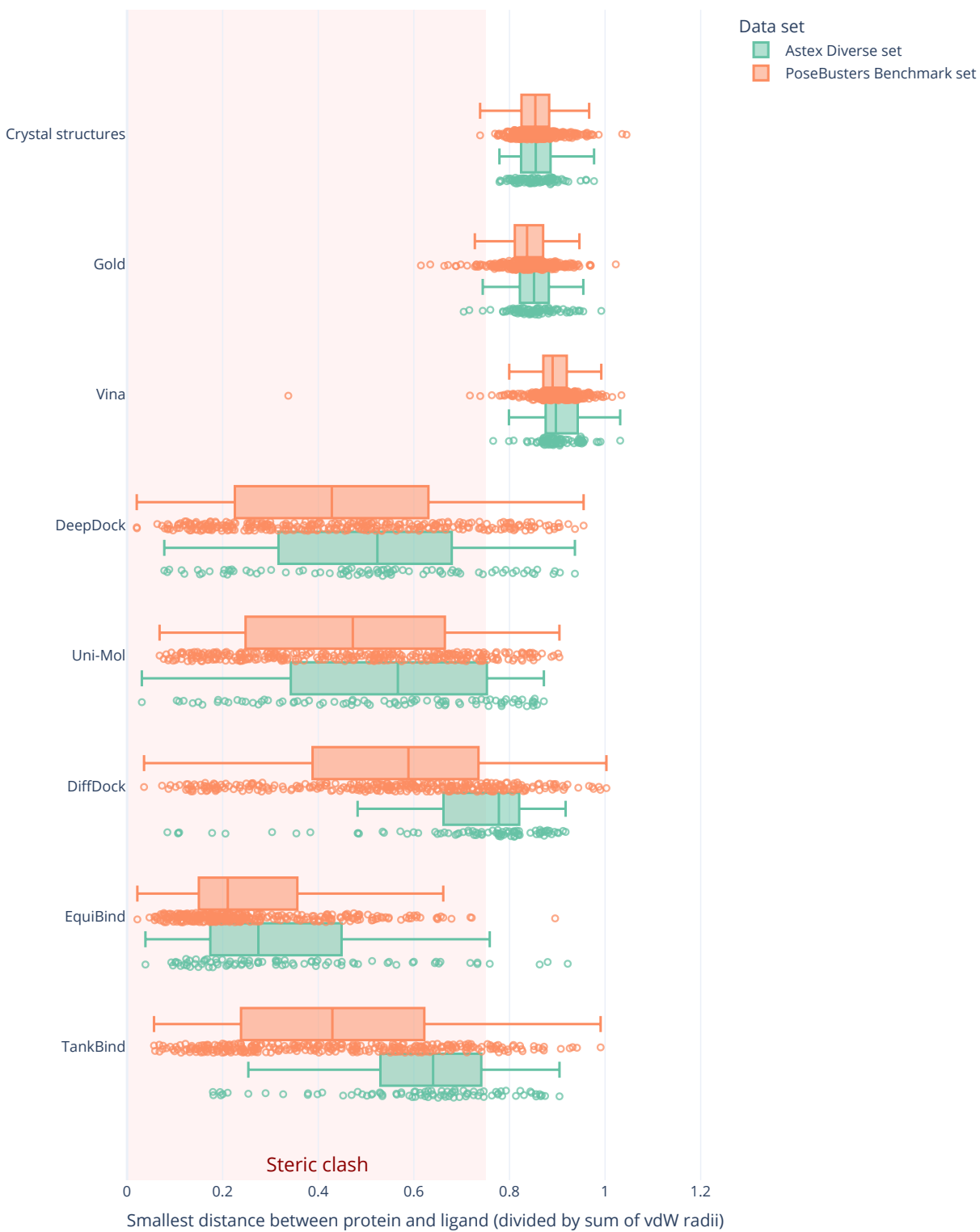


Figure S15: Minimum distances between protein and ligand. Distance is the smallest pairwise distance of heavy atoms of the ligand and protein normalized by their sum of van der Waals radii. The red area highlights the rejection zone below the cutoff of 0.75

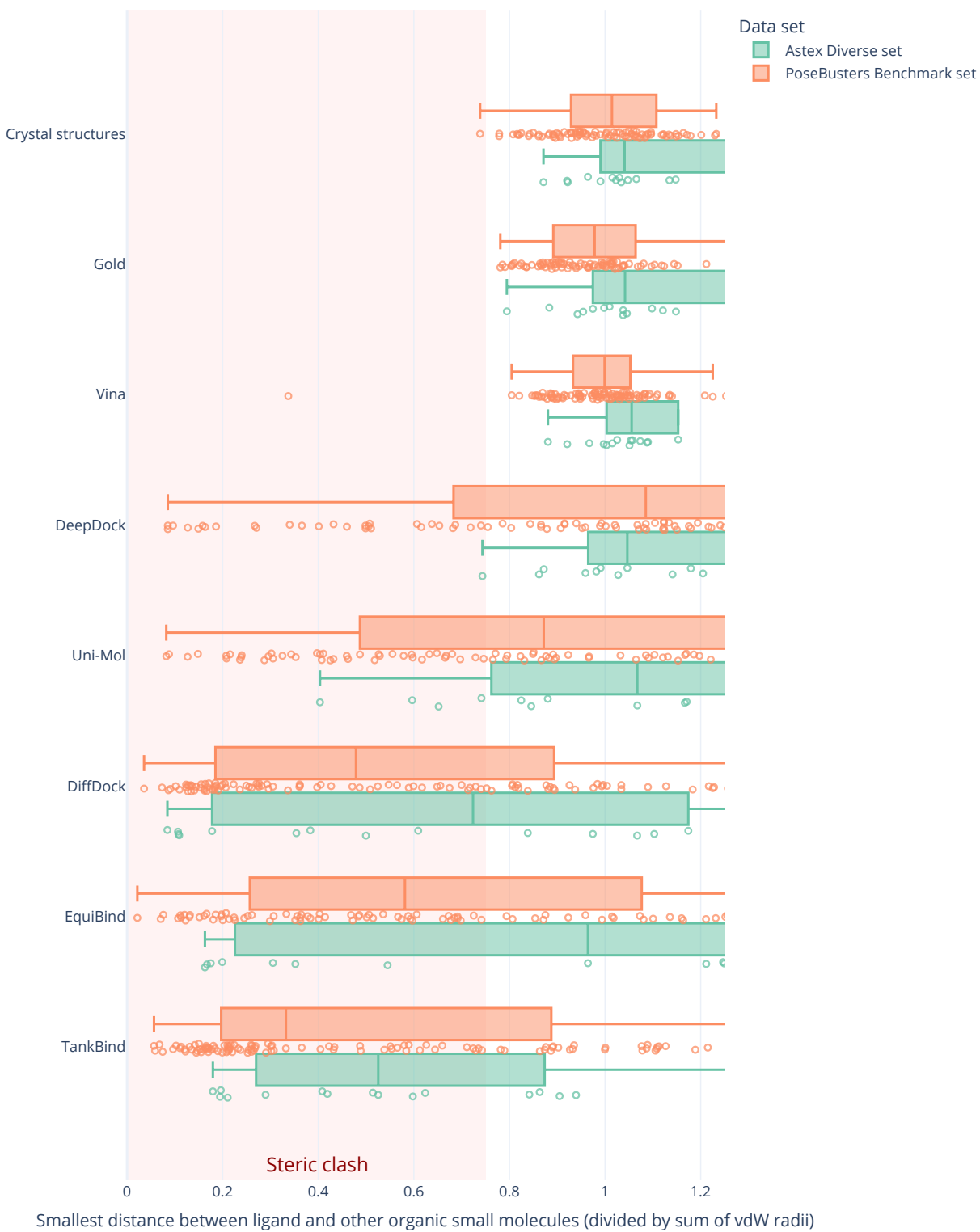


Figure S16: Minimum distances between ligand and organic molecules. Distance is the smallest pairwise distance of heavy atoms of the ligand and organic molecules normalized by their sum of van der Waals radii. The red area highlights the rejection zone below the cutoff of 0.75

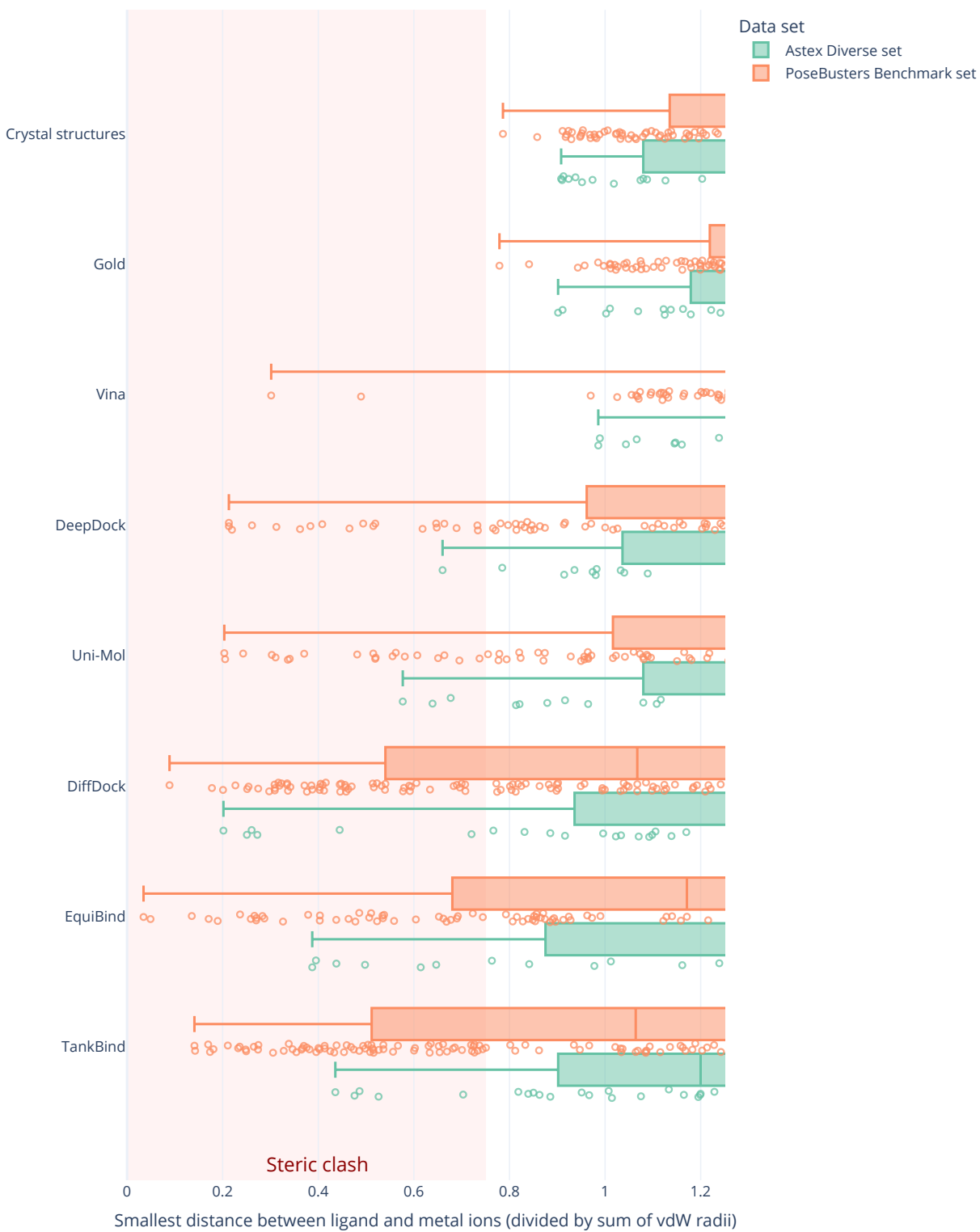


Figure S17: Minimum distances between ligand and inorganic cofactors. Distance is the smallest pairwise distance of heavy atoms of the ligand and inorganic cofactors normalized by their sum of covalent radii. The red area highlights the rejection zone below the cutoff of 0.75

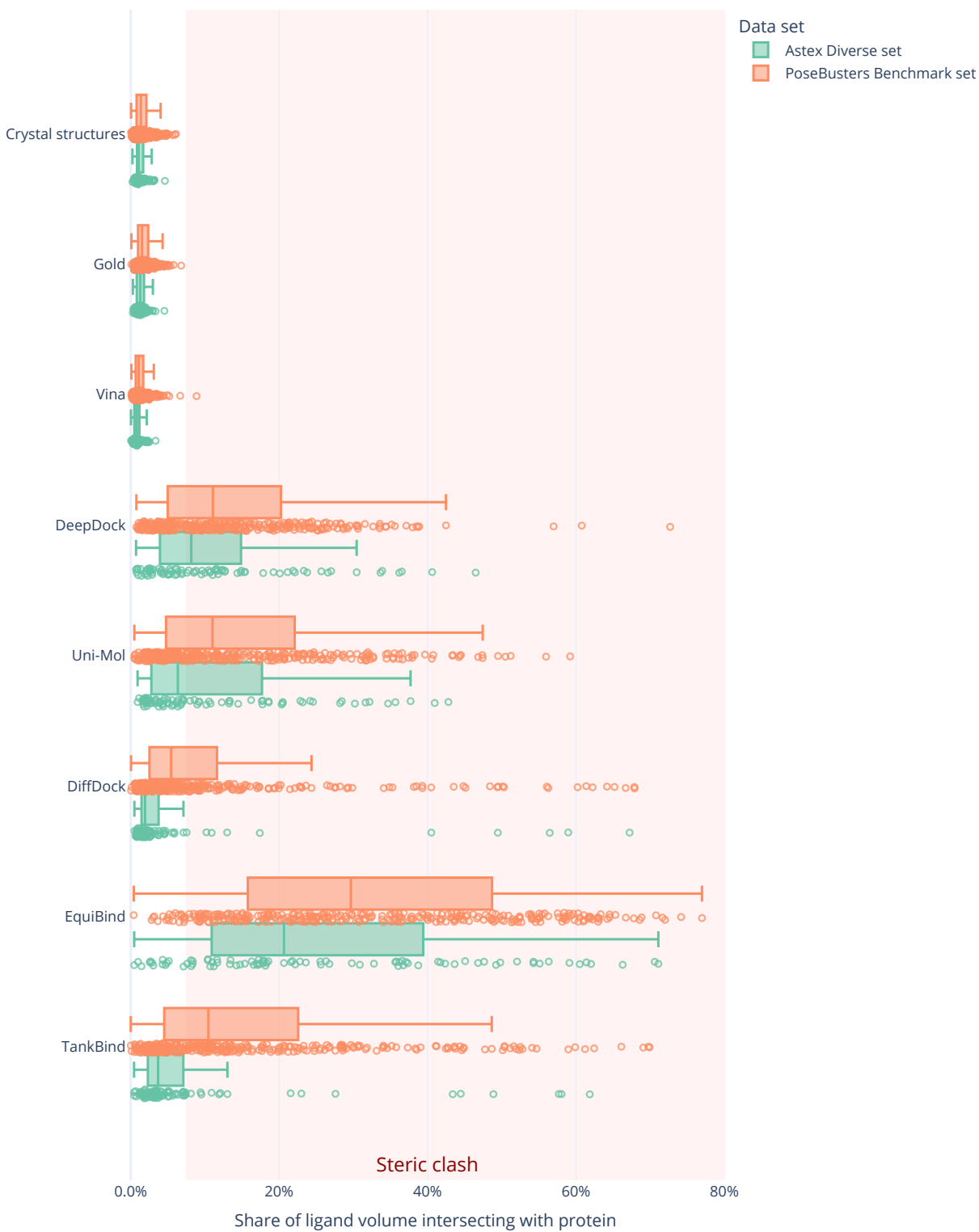


Figure S18: Volume overlap of protein and ligand. Volume overlap is the percentage of the ligand that overlaps with the protein. The volumes are the van der Waals volumes of the heavy atoms of the ligand and protein. The van der Waals radii are scaled by 0.8. The red dashed line shows the used cutoff of 5%.

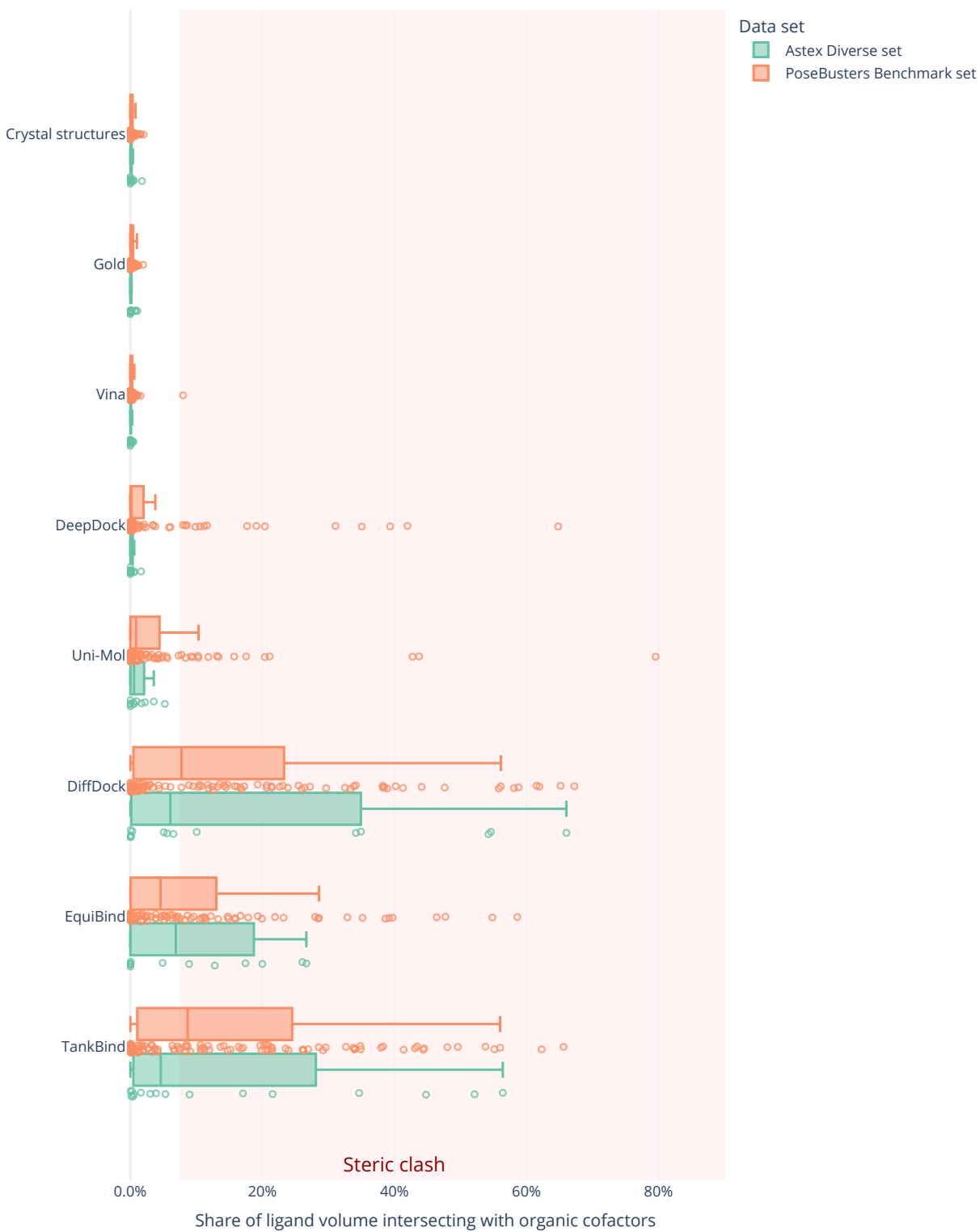


Figure S19: Volume overlap of ligand and organic molecules. Volume overlap is the percentage of the ligand that overlaps with the organic molecules. The volumes are the van der Waals volumes of the heavy atoms of the ligand and organic molecules. The van der Waals radii are scaled by 0.8. The red dashed line shows the used cutoff of 5%.

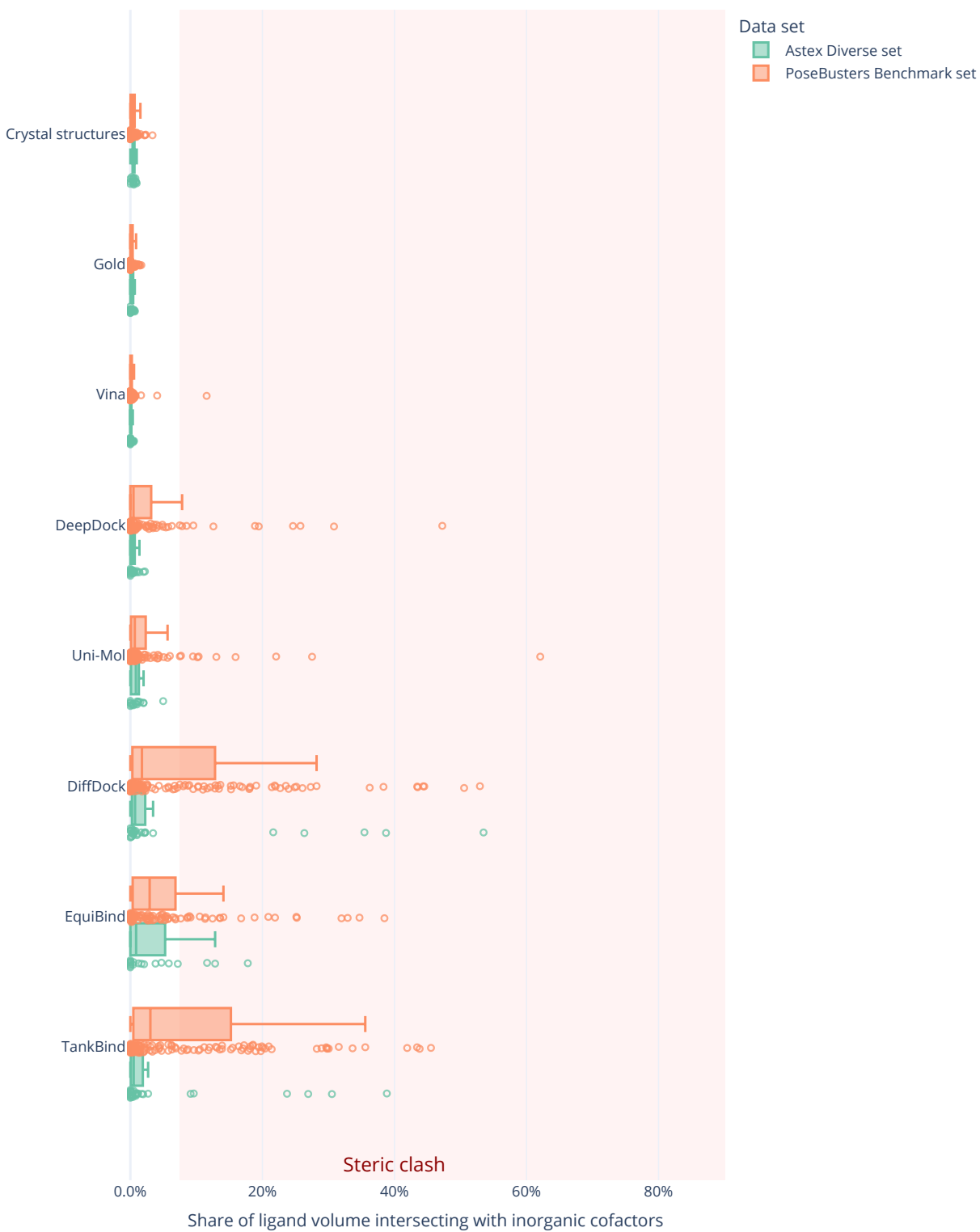


Figure S20: Volume overlap of ligand and metal ions. Volume overlap is the percentage of the ligand that overlaps with the metal ions. The volumes are the van der Waals volumes of the heavy atoms of the ligand and metal ions. The van der Waals radii are scaled by 0.8. The red zone shows the used cutoff of 20%.

Supplementary information references

- [1] S. Wang, J. Witek, G. A. Landrum and S. Riniker, *Journal of Chemical Information and Modeling*, 2020, **60**, 2044–2058.
- [2] P. Tosco, N. Stiefl and G. Landrum, *Journal of Cheminformatics*, 2014, **6**, 37.
- [3] S. Riniker and G. A. Landrum, *Journal of Chemical Information and Modeling*, 2015, **55**, 2562–2574.
- [4] G. Landrum, P. Tosco, B. Kelley, Ric, Sriniker, Gedeck, D. Cosgrove, R. Vianello, NadineSchneider, E. Kawashima, D. N, A. Dalke, G. Jones, B. Cole, M. Swain, S. Turk, AlexanderSavelyev, A. Vaucher, M. Wójcikowski, I. Take, D. Probst, V. F. Scalfani, K. Ujihara, G. Godin, A. Pahl, F. Berenger, JLVarjo, Jasondbiggs, Strets123 and JP, *RDKit Q3 2022 Release*, Zenodo, 2023.
- [5] B. Buchfink, K. Reuter and H.-G. Drost, *Nature Methods*, 2021, **18**, 366–368.
- [6] H. M. Berman, *Nucleic Acids Research*, 2000, **28**, 235–242.
- [7] J. D. Westbrook, C. Shao, Z. Feng, M. Zhuravleva, S. Velankar and J. Young, *Bioinformatics*, 2015, **31**, 1274–1278.